

Abstract

A high resolution simulation covering the Iberia–Biscay–Ireland (IBI) region is set-up over July 2007–February 2009. The NEMO model is used with a $1/36^\circ$ horizontal resolution on 50 z-levels in the vertical. It is forced by the astronomical potential and atmospheric forcing fields which consist of 3-hourly ECMWF analyses. Initial hydrographic conditions are derived from an Atlantic and Mediterranean Sea analyse at $1/12^\circ$ from Mercator Ocean (PSY2V3 model). At the open boundaries, IBI is forced with PSY2V3 temperature and salinity fields. It is also forced with tidal currents and elevations and inverse barometer elevations. In this study we evaluate the realism of the simulation through comparisons with an extensive observational dataset including climatology, temperature and salinity profiles, satellite SST data, sea surface buoys, tide gauges, altimeter data and HF radar data. A specific interest is given to the procedure used for the validation. General aspects of the simulation and its quality are analysed and particular attention is given to the validation of high frequency processes including the diurnal cycle, barotropic and internal tides, and surges. Finally, we focus on specific aspects of the circulation on the European sea shelves and give a qualitative assessment by studying tidal fronts, and specially the Ushant front, and the winter extension of the Iberian Poleward Current along the Northern Spanish coast during winter 2007–2008.

1 Introduction

The North East Atlantic (NEATL) region covers areas of important economic and social activities that include fisheries, transportation of oil and gas, commercial ship traffic, coastal management and protection and energy production. The increasing number of users over this region requires a good knowledge of the marine environment to suitably develop these activities. Regional modelling is a tool of particular interest required by this concern. The IBI system (Iberia–Biscay–Ireland) has been developed within this context. It aims at improving our knowledge of the circulation and our understanding

OSD

9, 499–583, 2012

NEMO on the shelf: assessment of the Iberia–Biscay–Ireland configuration

C. Maraldi et al.

Title Page

Abstract

Introduction

Conclusions

References

Tables

Figures

⏪

⏩

◀

▶

Back

Close

Full Screen / Esc

Printer-friendly Version

Interactive Discussion



NEMO on the shelf: assessment of the Iberia–Biscay–Ireland configuration

C. Maraldi et al.

Title Page

Abstract

Introduction

Conclusions

References

Tables

Figures



Back

Close

Full Screen / Esc

Printer-friendly Version

Interactive Discussion



of the dynamics in the NEATL region. The latter encompasses large scale physical processes but also local ones such as slope currents, coastal upwellings, fronts, river plumes and tides (barotropic and internal). In the deep ocean area, the near-surface large-scale circulation of the North Atlantic Ocean is primarily driven by the wind and is characterized by the anticyclonic North Atlantic sub-tropical gyre (Schmitz and Mc-
 5 Cartney, 1993). The main currents associated with the eastern part of this gyre are the North Atlantic Current and the Azores Current. They meet off West Iberia, a region also characterized by a poleward slope current flowing along the Eastern Atlantic margin in subsurface and still observed off Northwest Ireland (White and Bowyer, 1997). Over
 10 large shelf regions currents are dominated by tides. In the presence of stratification, interactions between tidal currents and strong bathymetry gradients generate internal tides that propagate onto the shelf and into the deep ocean (Pingree et al., 1986). Over the European continental shelf strong tidal currents also induce vertical mixing which creates thermal fronts between stratified and tidally mixed waters (Simpson and
 15 Hunter, 1974).

To ensure the realism of the model in a region that comprises a large spectrum of regimes specific to coastal, shelf, slope and deep ocean regions, a high resolution configuration is set up over the IBI region. We use the NEMO/OPA 9.0 model (Madec et al., 1998) in a realistic configuration, with a $1/36^\circ$ horizontal resolution and 50 z-levels in
 20 the vertical. As NEMO was originally developed for large scale modelling, new developments have been implemented to make it suitable for shelf and coastal modelling. In particular, missing physics have been added for the free surface, vertical mixing and bottom friction. The model now includes a tidal potential and 3-h atmospheric forcing which are likely to resolve the diurnal cycle and surges.

25 In this study, our objective is to define a methodology to assess the realism of the model that takes into account the specificities of the coastal dynamics and of the type of observations available in coastal and shelf seas. In particular, a new and challenging issue is the assessment of high-frequency dynamics, such as barotropic and internal tides, surges or circulation variability at daily time-scales. Our approach is inspired by

NEMO on the shelf: assessment of the Iberia–Biscay–Ireland configuration

C. Maraldi et al.

Title Page

Abstract

Introduction

Conclusions

References

Tables

Figures



Back

Close

Full Screen / Esc

Printer-friendly Version

Interactive Discussion

the strategy developed within the MERSEA European project (Le Provost et al., 2001). We demonstrate the feasibility of our methodology by applying it to the NEMO model in the IBI realistic configuration over the year 2008. This leads us to draw first conclusions on the ability of the model to represent the circulation over a broad range of spatial and time scales: from the large-scale of the deep ocean dynamics to the small scales on the slope and on the shelf, and from seasonal time scale to a few hour time scale.

This work was carried out within the MyOcean project, which aims at developing Marine Core Services within the GMES initiative (Global Monitoring for Environment and Security). One major activity within MyOcean is modelling and forecasting, both at global and regional scales where shelves are present. The assessment of numerical models in shelf areas is scientifically relatively uncharted territory, while being critical in a community approach where several teams and models are involved. Therefore our aim in this article is twofold: propose a set of diagnostics and metrics which could serve as a basis for community model assessment, and show their results for NEMO in its IBI implementation.

The paper is organized as follows. Section 2 focuses on the NEMO model and its new developments. It also describes the forcing, the input parameters, the model configuration and the experiment. Sections 3 to 6 provide an assessment of the model realism by investigating circulation, hydrological structures, SST, and barotropic and internal tides. In each section, data used for the comparisons are first presented and then we assess the model performances from large scales and low frequencies to high frequencies. In Sect. 7, we focus on specific processes in the Bay of Biscay. Temperature fronts induced by tidal mixing are analysed. In particular, we analyse the model quality in the Ushant front region by comparing vertical temperature section with observations collected during the MOUTON cruise. We also focus on a well-known pattern of the Bay of Biscay seasonal circulation: the winter warm extension of the Iberian Poleward Current along the Northern Spanish coast (Navidad event). The event of winter 2007–2008 is studied in detail. Finally, Sect. 8 gives a summary and conclusions.

2 Modelling

2.1 Numerical model

The IBI model numerical core is based on the NEMO v2.3 Ocean General Circulation Model (Madec et al., 1998; Madec, 2008). It solves the three dimensional primitive equations in spherical coordinates, discretized on an Arakawa C-grid, assuming hydrostatic and Boussinesq approximations. While the bulk of the numerical code is similar to the one described in Barnier et al. (2006) (including the vector invariant form of the momentum equations and the discretization of vorticity terms), there are important differences related to the specific coastal and tidal dynamics studied here that are briefly described in the following.

In order to allow fast external gravity waves, the “filtered” free surface formulation (Roullet and Madec, 2000) has been replaced by a time-splitting scheme: the barotropic part of the dynamical equations is integrated explicitly with a short time step while depth varying prognostic variables (baroclinic velocities and tracers) that evolve more slowly are solved with a larger time step. The mode coupling procedure as well as the barotropic scheme (a “generalized forward backward”) follow the work of Shchepetkin and McWilliams (2004) adapted to the standard NEMO leap-frog time stepping of “slow” varying variables.

Because of the explicit simulations of tides, sea level elevation can become large on the shelf compared to the local depth so that linear free surface approximation needs to be relaxed. In practice, the model vertical levels are remapped on the vertical to account for the varying fluid height. This has some important consequences on tracers’ conservation and on the generation of compound waves in shallow areas (Fanjul et al., 1997).

Vertical turbulent mixing processes are parameterized with a k-epsilon two-equation model implemented in the generic form proposed by Umlauf and Burchard (2002). The model is complemented with the type “A” full equilibrium form of Canuto et al. (2001) stability functions (all model parameters exactly follow Holt and Umlauf

NEMO on the shelf: assessment of the Iberia–Biscay–Ireland configuration

C. Maraldi et al.

Title Page

Abstract

Introduction

Conclusions

References

Tables

Figures



Back

Close

Full Screen / Esc

Printer-friendly Version

Interactive Discussion



Along lateral boundaries, free slip boundary conditions are used everywhere except inside Gibraltar strait where no slip conditions are applied. This somewhat reduces the flow to more realistic values and prevents the Alboran jet from turning into a quasi-permanent “coastal mode”. At the bottom, a quadratic bottom drag with a logarithmic formulation is calculated as:

$$C_d = \max\left(C_{d\min}, \left\{\kappa \ln(0.5\Delta z_b/z_0)\right\}^2\right) \quad (4)$$

Where $\kappa = 0.4$ is the Von Karman constant, $C_{d\min} = 2.5 \times 10^{-3}$ a minimum drag coefficient, Δz_b is the lowermost bottom cell thickness and $z_{0b} = 3.5 \times 10^{-3}$ m, the bottom roughness. With the reference geopotential discretization chosen here, the logarithmic formulation applies for depths shallower than 170 m, ie on most of the continental shelf.

Lateral sub-grid scale mixing are parameterized according to horizontal bi-harmonic operators for both momentum ($A_m = -2.5 \times 10^8 \text{ m}^4 \text{ s}^{-1}$) and tracers ($A_t = -2.5 \times 10^7 \text{ m}^4 \text{ s}^{-1}$), the latter value leading to particularly small explicit diffusion. Tracers' advection is computed with the QUICKEST scheme developed by Leonard (1979).

2.2 Model configuration

The model domain covers the North East Atlantic ocean from the Canary Islands to Iceland (Fig. 1). Even if the focus of the IBI forecasting system remains on the Iberian, French, and Irish coasts, the computational domain has been extended to include the Western Mediterranean Sea and the North Sea; this strategy was chosen to set connections with the global model where it suffers the less from not simulating the physical processes of interest here. Moreover, it allows for the explicit computation of mass, heat and salt fluxes in the narrow Gibraltar and Kattegat straits which may be better resolved due to the improved resolution. Also shown on Fig. 1 are the main surface features of the mean and transient circulation in the IBI area: the Azores Current (AC), the Canary Current (CaC), the Northern Current (NC), the Iberian Poleward Current

NEMO on the shelf: assessment of the Iberia–Biscay–Ireland configuration

C. Maraldi et al.

Title Page

Abstract

Introduction

Conclusions

References

Tables

Figures

⏪

⏩

◀

▶

Back

Close

Full Screen / Esc

Printer-friendly Version

Interactive Discussion



(IPC), the Norwegian Coastal Current (NwCC), the North Atlantic Current (NAC) as well as eddies in the Mediterranean Sea and in the Bay of Biscay.

The primitive equations are discretized on an horizontal curvilinear grid which is a refined subset at $1/36^\circ$ ($\sim 2\text{--}3$ km) of the so-called “ORCA” tripolar grid, commonly used in other NEMO based large scale and global modelling experiments (Barnier et al., 2006). This is also an exact 3:1 refinement of the North Atlantic model grid (PSY2V3 grid) that provides initial and boundary conditions. This strategy greatly simplifies interpolation procedures, allows for exact boundary fluxes/bathymetry matching, the latter increasing the overall robustness of the coupling. The same 50 reference z-levels as in the parent grid model are used in the vertical, with a resolution decreasing from ~ 1 m in the upper 10 m to more than 400 m in the deep ocean. A partial step representation of the very last bottom cell is used which improves the large scale circulation, but also gives a fairly smooth and accurate representation of the shelf bathymetry (Barnier et al., 2006).

The original bathymetry is derived from the 30 arcsec resolution GEBCO 08 data set (Becker et al., 2009) merged with regional bathymetries provided by Ifremer, the French Navy (SHOM, Service Hydrographique et Océanographique de la Marine) and the North West Shelf Operational Oceanographic System (NOOS). Local bathymetric grids cover the Mediterranean Sea, the Gibraltar Strait, regions off Portugal and off North Spain, regions along the French coasts, the Southern Celtic Sea, part of the North Sea and the Baltic Sea. Independent ICES (International Council for the Exploration of the Sea) soundings have been used to validate the new bathymetry dataset. Significant improvements have been achieved in shelf sea regions in comparison to the original GEBCO08 bathymetry (Fig. 2). The model bathymetry is then bilinearly interpolated from the resulting composite and slightly smoothed using a Shapiro filter to remove grid scale noise and remaining discontinuities between local databases. At open boundaries, within 30 points wide relaxation areas, bathymetry is exactly set to the parent grid model bathymetry and progressively merged as a 7 point sine with the interpolated dataset described above.

**NEMO on the shelf:
assessment of the
Iberia–Biscay–Ireland
configuration**

C. Maraldi et al.

Title Page

Abstract

Introduction

Conclusions

References

Tables

Figures



Back

Close

Full Screen / Esc

Printer-friendly Version

Interactive Discussion



2.3 Forcing

Meteorological fields from the European Centre for Medium-Range Weather Forecasts (ECMWF) with a 3-h period and $0.25^\circ \times 0.25^\circ$ horizontal resolution are used to force the model. According to Bernie et al. (2005), this temporal resolution associated with adequate vertical resolution in surface layers (typically one meter as used here or less) is sufficient to model diurnal variations of SST. Evaporation, turbulent heat fluxes and wind stresses are computed according to Large and Yeager (2004) bulk formulae.

Since the model domain encompasses areas with very different optical water properties (from highly turbid on the shelf to clear waters in the subtropical gyre), a spatially variable solar penetration depth is used. It is built from a 10 yr, 9 km, monthly climatology of Seawifs satellite data. In practice, we use the diffusive attenuation coefficient at 490 nm (kd_{490}) which is transformed into an equivalent photosynthetically attenuation coefficient K_{par} according to Morel et al. (2007):

$$K_{par} = 0.0665 + 0.874kd(490) - 0.00121/kd(490) \quad (5)$$

This methodology and the different algorithm used for the retrieval of attenuation from satellite data are nevertheless only valid for Case-1 waters (where chlorophyll concentration controls optical properties). As a correction, Seawifs based estimate is merged with a monthly climatology processed by Ifremer (Gohin et al., 2005) which is valid in coastal waters. The K_{par} threshold value between Case-1 and Case-2 waters (over which Ifremer data only is considered) has been set to 0.12 m^{-1} .

At 33 major rivers mouths, climatological monthly flow-rates are prescribed (Fig. 3). These have been obtained by averaging data from the Global Runoff Data Center (<http://grdc.bafg.de>) and the French hydrographic database “Banque Hydro” (<http://hydro.eaufrance.fr>). No shearing of the input velocity profiles nor temperature fluxes are considered.

After numerous tests, relatively simple, yet robust formulations have been chosen as open boundary schemes: Blayo and Debreu (2005) characteristic method for barotropic variables (elevation and transports) and clamped conditions for baroclinic

OSD

9, 499–583, 2012

NEMO on the shelf: assessment of the Iberia–Biscay–Ireland configuration

C. Maraldi et al.

Title Page

Abstract

Introduction

Conclusions

References

Tables

Figures

⏪

⏩

◀

▶

Back

Close

Full Screen / Esc

Printer-friendly Version

Interactive Discussion



velocities, temperature and salinity. For the latter variables a 30-points relaxation area with a minimum time-scale of 1 day is used which strongly damps outgoing perturbations from the prescribed fields while allowing for the explicit simulation of high frequency fluctuations related to the atmosphere in the surface layers.

5 Temperature, salinity, velocities and sea surface height (hereafter SSH) from PSY2V3 daily outputs are used as the slow component of open boundary data. PSY2V3 is an operational forecasting system covering the North Atlantic and the Mediterranean Sea at $1/12^\circ$ resolution. It does include a multivariate, Kalman based, weekly data assimilation procedure of along track altimetry data, sea surface temperature (SST) and hydrological observations (Dréville et al., 2008; Dombrowski et al., 10 2009). SSH tidal forcing is then added as the sum of 11 constituents (M_2 , S_2 , K_2 , N_2 , K_1 , O_1 , P_1 , Q_1 , M_4 , M_f , M_m) provided by the TPXO7.1 global tide model (Egbert et al., 1994). A 35 days barotropic experiment (e.g. without stratification) with clamped boundary conditions for sea level (and Neumann conditions for velocities) is used to 15 estimate the 6 major barotropic tidal velocities constituents (similar to the run_{bt} experiment described in the following). This method, reminiscent of the iterative procedure of Flather, 1987, clearly improved the overall tidal statistics compared to direct use of TPXO velocity data for all constituents. Finally, since surface atmospheric pressure forcing is explicitly considered in the dynamical equations, approximate sea level re- 20 sponse in the inverse barometer form is added to sea level data.

2.4 Experimental set-up

Results from two simulations are considered in the following: a “tide only” run (experiment T91, hereafter run_{bt}) which consists in a 35 day “barotropic-like” simulation (homogenous density, no atmospheric forcing, only tidal forcing) is used to perform 25 a 3-D harmonic analysis that provides tidal elevations and currents for a reduced set of harmonics (M_2 , S_2 , N_2 , K_1 , O_1 , Q_1 , M_4), and a second simulation (experiment T102, run_{bc}) is run with stratification but the harmonic analysis is only performed onto sea surface currents and vertical profiles at buoy locations (see Table 1). In the latter case,

NEMO on the shelf: assessment of the Iberia–Biscay–Ireland configuration

C. Maraldi et al.

Title Page

Abstract

Introduction

Conclusions

References

Tables

Figures



Back

Close

Full Screen / Esc

Printer-friendly Version

Interactive Discussion



the model is initialized on 25 July 2007 from analysed temperature, salinity, sea level and velocities bilinearly interpolated from PSY2V3 analysis. Tidal and surface pressure forcings are smoothly introduced (both at open boundaries and in dynamical equations) thanks to a 2 days linear ramp. Meanwhile, horizontal viscosity linearly decreases from 4 times its nominal value, to damp instabilities arising from the use of unbalanced initial fields. The simulations ends in February 2009. Model analysis shown hereafter concerning year 2008 only.

3 Assessment of the circulation

3.1 Surface eddy kinetic energy

As a first check of the model self-consistency, we analyse the eddy kinetic energy (EKE). Note that the investigation of the EKE is not part of the so-called metrics but is a necessary step to assess the model quality. The EKE distribution gives good indications of the ocean dynamics in our region of study. Maps of surface EKE are computed using hourly velocity fields and are presented in Fig. 4 for periods shorter and longer than 25 h. Filtering at 25 h is a standard processing to separate high frequency signal such as tides from the lower frequency dynamical effects. Strong values of the high frequency EKE (HFEKE) are located on the European continental shelf where tides are particularly large and contribute to most of the HFEKE (Van Aken, 2002). In particular, the highest values of EKE are located in the English Channel, in the Irish Sea, off Southeast English coasts, in the German Bight, North of Scotland and around the Faeroe Islands where tidal currents are the most important (Davies et al., 1997; Holt et al., 2001). On the European shelf seas, regions of separation between low and high HFEKE, as the entrance of the English Channel or in the Irish Sea, correspond to well identified tidal front locations (Bowers and Simpson, 1987; Holt and Umlauf, 2008). Over the Armorican shelf, at 48° N, we clearly distinguish bands parallel to the shelf break due to successive maxima and minima of HFEKE. The distance between

NEMO on the shelf: assessment of the Iberia–Biscay–Ireland configuration

C. Maraldi et al.

Title Page

Abstract

Introduction

Conclusions

References

Tables

Figures

⏪

⏩

◀

▶

Back

Close

Full Screen / Esc

Printer-friendly Version

Interactive Discussion



NEMO on the shelf: assessment of the Iberia–Biscay–Ireland configuration

C. Maraldi et al.

Title Page

Abstract

Introduction

Conclusions

References

Tables

Figures

⏪

⏩

◀

▶

Back

Close

Full Screen / Esc

Printer-friendly Version

Interactive Discussion

two crests is about 30 km which is similar to the M_2 internal tide wavelength in this region (Pairaud et al., 2010) and supports that the HFEKE pattern corresponds to the propagation of internal tides from the slope to the coast. Over the abyssal plain, HFEKE is relatively small in comparison with the shelf regions (Le Hénaff et al., 2009).

5 However some areas, as off Northwestern Iberia, present higher values. These areas correspond to strong bathymetric gradient areas where internal tides may be generated on the slope and induce higher HFEKE. This hypothesis tends to be confirmed by larger values of HFEKE in summer than in winter in these regions (not shown) due to the seasonal stratification which increases internal tides signals. High HFEKE also occurs
10 in the Gibraltar Strait where tidal currents are large and highly variable (Candela et al., 1990; Sannino et al., 2004). In the Bay of Biscay, the spatial distribution of HFEKE is similar to the one obtained by Van Aken (2002) from drifters data but with larger magnitudes. This author used 3 h velocity fields for the HFEKE computation and may underestimate it.

15 At lower frequencies the values of surface EKE are smaller than HFEKE values. At longer time scales, oceanic processes contributing to the ocean dynamic variability are eddies and current variability. In the Mediterranean Sea high EKE is found in regions of strong mesoscale activity such as the Alboran Sea and along the Algerian coast (Pujol and Larnicol, 2002). It is also associated with the variability of the Northern
20 Current along the French and the Spanish continental shelf slope (Rubio et al., 2009), winter deep convection (Herrmann et al., 2008), and, as far as continental shelves are concerned, by river water discharges (Reffray et al., 2004). In the Atlantic part of the domain the EKE is much lower than in the Mediterranean Sea. It shows clear meridional variations with low values south of 50° N except between 35° N and 40° N,
25 at the Azores Current (AC) latitudes, and higher values in the northern basin. Off Western Iberia and in the Bay of Biscay EKE is relatively weak. Along Western and Northern Iberian coasts, higher EKE magnitudes are associated with variability of the Iberian Poleward Current (IPC). In the abyssal plain of the Bay of Biscay, higher EKE is mainly due to the westward propagation of slope water eddies (SWODDIES; Pingree

that the circulation is properly modelled in the region (Otto et al., 1990; Rydberg et al., 1996; Rodhe, 1996). The Norwegian Coastal Current transports 1.23 Sv in the model which is consistent with values from Otto et al. (1990).

3.3 Focus on transports at the Gibraltar Strait

5 The transport through the Strait of Gibraltar is controlled by various processes at different time scales. Among these processes tides are the most energetic influencing the mean flow (Tsimplis and Bryden, 2000). Thus hourly transport through the Gibraltar Strait has been computed to analyse the outflow variability. Following the study of Sánchez Román et al. (2009) the interface to separate the inflow from the outflow
10 has been computed as the time dependent depth of the surface of zero low-pass frequency velocity. The modelled outflow transport estimated with this interface is noted $Q_{mod,V}$. The outflow transport computed using the commonly used 37.25 isohaline ($Q_{mod,S}$) is also computed for comparisons. Fig. 6 illustrates time series of observed and modelled transports and also the depth of the interface for $Q_{mod,V}$ and $Q_{mod,S}$
15 over a period overlapping the model simulation and the transport estimates of Sánchez Román et al. (2009), noted $Q_{obs,V}$. The definition of the interface based on the depth of the zero velocity gives better results than the isohaline interface. In comparison to the $Q_{obs,V}$ mean transport of -0.72 Sv, the mean outflow of $Q_{mod,V}$ is -0.74 Sv and the correlation coefficient with $Q_{obs,V}$ is 0.71, while a lesser agreement is found for
20 $Q_{mod,S}$ with a too small transport of -0.69 Sv and a correlation coefficient of 0.66. The time series of the $Q_{mod,V}$ associated interface presents strong oscillations that can reach up to 40 m. Its mean depth is 181 m over the period. The $Q_{mod,S}$ interface presents more pronounced fortnightly oscillations with deeper values reached during neap tides. The $Q_{mod,V}$ has also a strong fortnightly variability with maximum outflow
25 values during spring tides. Differences between peak values and lower values at neap tides reaches 0.70 Sv both in $Q_{obs,V}$ and $Q_{mod,V}$.

NEMO on the shelf: assessment of the Iberia–Biscay–Ireland configuration

C. Maraldi et al.

Title Page

Abstract

Introduction

Conclusions

References

Tables

Figures

⏪

⏩

◀

▶

Back

Close

Full Screen / Esc

Printer-friendly Version

Interactive Discussion



3.4 Residual sea surface elevation

The in situ sea level dataset consists in 115 tide gauges located along the European coasts (Fig. 1). Tide gauge data used for comparisons are provided by Puertos del Estado, the Marine Institute and the Danish Meteorological Institute; data from SHOM, BODC (British Oceanographic Data Center) and GLOSS provided by CLS via the Badomar specific database are also used (see red dots on Fig. 1). Residual elevations (e.g. detided sea levels) are used to diagnose the model performance at different time scales. Comparisons between residual elevations from the model and the observations are shown in Fig. 7. The elevations due to the IB effects have been added to the comparison. This classical correction corresponds to the static response of the ocean to atmospheric pressure while the model residual elevations also include the non static response and the elevations due to wind forcing effects. The model shows very good agreement with data over the whole domain and it performs better than the IB response. However this result strongly depends on the latitude and the frequency band. The model is the most effective at high latitudes which are more energetic areas and where the ocean dynamical space and time scales are smaller, while at mid latitudes the model response to atmospheric forcing is closer to the IB approximation. Besides, the ocean response to atmospheric pressure generally differs from the IB at periods below 3 days (Carrère and Lyard, 2003) and we observe that for longer periods the IB performance and the model performance are very similar at mid latitudes (Fig. 7c shown for periods larger than 10 days). On the other hand, for periods below 10 days where wind effects prevail, the model is clearly more relevant over the whole domain. We also notice that model results are in a lesser agreement with data at low frequencies. At these frequencies the elevations signal is dominated by steric effects which are not represented in the model.

3.5 Residual currents

Data used for comparisons of residual currents consist in surface buoys provided by Puertos del Estdo and data provided by AZTI off Cabo Matxixako and San Sebastian on the Basque Country coasts that include current records between 10 m and 150 m and allow comparisons of residual currents along the water column depth (Table 1).

Wind stress observed at the buoy station and extracted from the model forcing using ECMWF wind fields is presented for the Estaca de Bares buoy station (Fig. 8). Wind stress has the same distribution in data and in forcing fields. It shows predominant zonal orientation but magnitudes are significantly higher in the ECMWF fields especially during strong wind events. The distribution of modelled residual currents is in good agreement with observations. Surface currents are mainly oriented zonally with axes slightly to the right of the wind axes attesting for the importance of the wind driving forcing on the residual currents. Nevertheless, there are noticeable discrepancies in the distribution: observations show non negligible meridional current components that are weak in the model. The depth as measured at the data location is 382 m while it is 405 m in the model bathymetry. Local discrepancies in the bathymetry and particularly in the representation of slope may explain the differences in the modelled dynamics. There are also differences in the current amplitudes that are overestimated in the model. This may be a direct consequence of overestimated wind stress magnitudes in the forcing.

Figure 9 shows observed and modelled current speed at the Matxixako location (AZTI data). Current magnitudes are of the same order in the data and in the model. They show short intensifications during winter that are associated with an eastward flow. The intensifications are underestimated in the model. In summer, the currents are weaker. Some current pulses are also distinguished in the data from June to September 2008 and are well reproduced in the model. The currents are well mixed in winter and stratified in summer both in data and in model. Comparison with thermohaline properties at the same station (Fig. 10) suggests that vertical shear is not sufficient to

**NEMO on the shelf:
assessment of the
Iberia–Biscay–Ireland
configuration**

C. Maraldi et al.

Title Page

Abstract

Introduction

Conclusions

References

Tables

Figures



Back

Close

Full Screen / Esc

Printer-friendly Version

Interactive Discussion



destruct the strong seasonal stratification (Rubio et al., 2012). At last, note that as the depth at the Matxitxako buoy location is 550 m in the data (observations are recorded over the first 200 m) and 780 m in the model, which means a slightly different location of the North Iberia continental slope. This difference is expected to induce model-data discrepancies.

4 Assessment of water masses and stratification

4.1 Climatology and profiles data

The “Analyse, Reconstruction et Indicateurs de la Variabilité Océanique” (ARIVO) climatology is a global climatology covering latitudes from 77° S to 77° N (von Schuckmann et al., 2009). It is a synthesis of ARGO array and profiling floats (www.argo.net) representing 95 % of the data, and drifting buoys, CTD and moorings over 2003–2008. An optimal analysis was performed with a radius of influence bounded at 300km and varying proportionally to the radius of Rossby with respect to the different scales of the dynamics in the shelf regions and in the abyssal plain. The resulting climatology provides monthly temperature and salinity fields on a 0.5° horizontal Mercator isotropic grid and on 152 standard levels between 0 m and 2000 m. Mean θ –S diagram derived from the climatology are compared to the model to ensure that the main water masses of the region of study are correctly rendered in the model.

Subsurface ocean temperature and salinity profiles from the UK MetOffice EN3 data set are used to assess the model hydrology in realistic conditions. The data are obtained from the World Ocean Database 2005 (Boyer et al., 2006), the Global Temperature and Salinity Profile Project and the Argo Project. They are quality controlled using a comprehensive set of checks (Ingleby and Huddleston, 2007). For each profile, mean bias and RMS between observations and model are computed. Comparisons of the mixed layer depth are also performed. We also use data from the two deep sea buoys of AZTI-Tecnalia (Rubio et al., 2012, Fig. 1, Table 1); they provide measurements of

NEMO on the shelf: assessment of the Iberia–Biscay–Ireland configuration

C. Maraldi et al.

Title Page

Abstract

Introduction

Conclusions

References

Tables

Figures



Back

Close

Full Screen / Esc

Printer-friendly Version

Interactive Discussion



scheme that generates spurious extremis. Below the MW, the deep layers envelope the Labrador Sea Water (LSW) characterized by a salinity minimum, the Eastern North Atlantic Deep Water (ENADW) identified by a relatively deep salinity maximum which is weaker in the model than in the climatology, the Iceland-Scotland Overflow Water (ISOW), the Lower Deep Water (LDW) originating from modified Antarctic Bottom Water, and the cold Denmark Strait Overflow Water (DSOW). The modelled thermohaline properties of the deep and bottom waters are in reasonable agreement with the climatology.

4.3 Rossby radius of deformation

To verify that biases in temperature and salinity do not introduce errors on the physical process representation we have computed the first Rossby radius of deformation (λ_1) using the formula published in Chelton et al. (1998) computed from yearly averaged hydrological fields of the climatology and the model (Fig. 12). In this formula, the Brunt-Vaisala frequency N is integrated over the whole water column. The Rossby radius decreases from ~ 27 km at 30° N to ~ 10 km at 60° N. The lower values between 35° N and 44° N are due to shallower regions at these latitudes. The Rossby radius is larger by up to 15% in the model. However, we know that for depth deeper than 1500 m, the climatology is less accurate than in shallower layers as it incorporates less temperature and salinity profiles. Thus we have integrated the formula presented in Chelton et al. (1998) over the upper 1500 m (Fig. 12b). The values of λ_1 obtained with the model are very close to climatological values. The integration of the hydrological properties over the water column depth (first 1500 m) smoothes out discrepancies in the MW core depth and the model shows a good realism for the representation of the dynamical processes studied in this paper.

NEMO on the shelf: assessment of the Iberia–Biscay–Ireland configuration

C. Maraldi et al.

Title Page

Abstract

Introduction

Conclusions

References

Tables

Figures



Back

Close

Full Screen / Esc

Printer-friendly Version

Interactive Discussion



4.4 Temperature profiles and mixed-layer depth

Figure 13 represents the RMS of the model-data misfits in temperature over the upper 200 m and the mixed layer depth (MLD) computed from the model and EN3 profiles. Results are shown for two months with different stratification: February, with deeper MLD due to strong mixing during winter period, and August with a more stratified water column. About the spatial distribution during these months, note that in August more profiles are available over the European shelf. In February, modelled temperatures show very good agreement with data almost everywhere over the upper 200 m (RMS globally lower than 0.5°C). The profile of temperature RMS computed over the whole IBI domain (not shown) indicates that maximum RMS values are reached between 50 m and 130 m which is consistent with differences in modelled and observed MLD distribution at these depth ranges (Fig. 13c). During August the water column is more stratified. Larger RMS in temperature profiles (up to 2°C) are found on shelves as well as in the deep ocean. The model globally overestimates the temperature over the upper 200 m in the deep ocean, in the Iroise Sea and the English Channel. In the North Sea, larger RMS values are associated with warm as well as cold bias. Discrepancies between the model bathymetry and the observed bathymetry are possible source of errors in this shallow water region. Another possible source of error may be the wave mixing parameterization coefficient. Sensitivity experiments performed with a $1/12^{\circ}$ resolution configuration have shown that the modelled MLD (and consequently temperatures in the upper ocean layers) is very sensitive to the wave mixing parameterization coefficient. The model MLD representation can be enhanced by tuning this parameter but the parameterization seems to be inadequate in semi-enclosed seas as the Mediterranean Sea or the North Sea. Thus the parameter used is a compromise to minimize the MLD errors both in the open ocean and in the semi-enclosed seas. The maximum RMS is found between 20 m and 60 m (the temperature RMS reaches nearly 1.1°C at 30–35 m), which correspond to the MLD value ranges over the region during August. The MLD distribution shows that modelled MLD is underestimated and

NEMO on the shelf: assessment of the Iberia–Biscay–Ireland configuration

C. Maraldi et al.

Title Page

Abstract

Introduction

Conclusions

References

Tables

Figures



Back

Close

Full Screen / Esc

Printer-friendly Version

Interactive Discussion



may result in warmer temperature profiles in the upper layers. In the model, wave-induced mixing, which is incorporated through a parameterization, is underestimated when wind stress is too weak. In winter, winds are strong and mixing is correctly modelled but in summer wind stress is weaker causing too small wave-induced mixing and underestimated MLD in the modelled.

4.5 Local stratification off the Basque country

The time evolutions of temperature and salinity as observed and modelled at the Matxitxako station ($43^{\circ} 37.9' N/2^{\circ} 41.6' W$) are presented in Fig. 10. The profiles show clear seasonal stratification which is a typical pattern of shelf region away from frontal zones. The model reproduces well the rapid heating and freshening of spring 2008. The cooling and mixed-layer deepening during winter are also correctly represented. However the model underestimates the MLD-equivalent in winter (the MDL-equivalent is computed as the depth at which the density changes from the density at 10 m is 0.01). This underestimation may be linked to uncertainties in the previous section. In summer 2007 we also notice that the model salinity is too low in the upper layers. This is due to the initialization from PSY2V3 which is too fresh in this region. On the contrary the model is slightly saltier in the surface layers during summer 2008. This may be due to river runoffs northeast of Spain which induce low salinity buoyant surface waters and which are not included in the model. However, note that rapid freshening pulses during September 2008 are well represented in the model. In November 2007, a rapid cooling of surface layers appears over a few day period. This event corresponds to an upwelling and is well reproduced in the model. During winter 2007–2008, the ocean becomes warmer and saltier over the whole water column. This phenomenon is more marked in the model and affects the 350 m upper layer. It corresponds to a warm extension of the Iberian Poleward Current (IPC) also called “Navidad event” (Frouin et al., 1990). The winter 2007 Navidad occurrence is studied in Sect. 7.

NEMO on the shelf: assessment of the Iberia–Biscay–Ireland configuration

C. Maraldi et al.

Title Page

Abstract

Introduction

Conclusions

References

Tables

Figures

⏪

⏩

◀

▶

Back

Close

Full Screen / Esc

Printer-friendly Version

Interactive Discussion



5 Assessment of SST spatial distribution and diurnal cycle

5.1 SST datasets

We used SST processed at Météo-France/CMS (Le Borgne et al., 2011) for comparisons with the model SST. The data consist in L3 multi-sensors products built from bias-corrected L3 mono-sensor products based on AATSR, METOP, NAR, AVHRR, SEVIRI, AMSRE, TMI and MODIS sensors. SST satellite data consists in daily produced fields covering the 40° W/55° E–20° N/70° N region with a 0.02° resolution and an accuracy of 0.5 °C. These data are used to assess the model ability at reproducing SST both in the deep ocean and in shelf regions. Statistical comparisons are made over a one year period.

The in situ buoy datasets include near surface observations of atmospheric pressure, air and sea surface temperature and, on some platforms, wind speed, wind direction and sea surface currents. They are provided by 4 networks: Puertos del Estado on the Spanish Shelf, Météo France on the Armorican shelf slope, in the Iroise Sea and in the Mediterranean Sea, and the Marine Institute on the Porcupine Bank and in the Celtic Sea (Fig. 1, Table 1). The dataset consists in hourly time series which enable the computation of the diurnal cycle. Our metrics using buoys data rely on time series comparisons and aim to evaluate the behaviour of the system at high frequencies (diurnal cycle) and at seasonal scales.

5.2 SST spatial distribution

For the SST comparisons, the model outputs were interpolated onto the data grid using tools adapted from Juza (2008). Model and data fields were monthly averaged to avoid spatial data gaps. Figure 14 represents maps of seasonally averaged SST and time series of monthly averaged bias and RMS between regional SST data and model SST for the year 2008. Maps of monthly bias show discrepancies that are significantly higher during summer months where it exceeds 0.6 °C (Fig. 14e). This is due to strong

OSD

9, 499–583, 2012

NEMO on the shelf: assessment of the Iberia–Biscay–Ireland configuration

C. Maraldi et al.

Title Page

Abstract

Introduction

Conclusions

References

Tables

Figures

⏪

⏩

◀

▶

Back

Close

Full Screen / Esc

Printer-friendly Version

Interactive Discussion



5.3 Low-frequency SST variability

Figure 16 represents a Taylor diagram of the observed and modelled SST at buoy locations. Concentric circles with the axis origins as centre represent the time series standard deviations which have been normalized by the observation values (e.g. data standard deviation is 1). Radius indicate the correlation and circles with the (1,0) origin represent the RMS difference between model and data. SST time series have been previously 1-day low pass filtered to remove the diurnal cycle signal which is discussed separately in Sect. 5.4. SST is particularly well modelled with “normalized” standard deviation close to 1 and correlation greater than 0.95 (except at Cabo Silliero and Vilano Sisargas where the correlation coefficients are 0.85 and 0.89, respectively). When looking regionally, stronger discrepancies are found for the Canary Island buoys where the simulated variability is overestimated by more than 15%. At Tenerife buoy station, the modelled SST is warmer than the observed SST all over the year 2008 (about 0.5 °C). Along the Armorican slope and within the Gulf of Cadiz, larger discrepancies are found due to overestimated modelled SST during summer. This is consistent with errors obtained in Fig. 14c in these regions. Warmer model SST during summer at these locations leads to a larger seasonal amplitude and to a higher variability at low frequencies.

5.4 Diurnal cycle

The diurnal cycle of SST (Dsst from herein) is generated by the daily variations of atmospheric fluxes. The Dsst amplitudes are computed over a 24 h period as the difference between the maximum SST and the minimum SST previously corrected from the daily trend (Pimentel et al., 2008). The Dsst for the buoy data are only computed when the 24 SST values per day are available to avoid any miscalculations of the Dsst amplitudes. Figure 17 displays box plots of the observed and the modelled Dsst amplitudes over the whole domain; it illustrates the distribution of data by showing different values of Dsst amplitudes below which a certain percentage of data are observed. Globally

Dsst amplitudes are underestimated in the model and the median observed Dsst is 0.25 °C while the median modelled Dsst is only 0.20 °C. When looking regionally at the distribution, we found that Dsst is underestimated almost everywhere for the 50 % of the data with smaller amplitudes (e.g., Dsst amplitudes below the median value). In the Mediterranean Sea, Dsst amplitudes are underestimated for all data and for all ranges of Dsst amplitudes. The resolution of the model and of the forcing, the surface heat fluxes and the vertical mixing in the upper ocean are critical aspects for the diurnal cycle modelling and may explain discrepancies between the observed and the modelled Dsst (Bernie et al., 2005; Pimentel et al., 2008). According to Bernie et al. (2005), a minimum of a 1 m vertical resolution in the upper ocean and of a 3 h temporal resolution of surface fluxes is required to resolve 90 % of the observed Dsst. The model is forced with 3 h atmospheric fields but has a coarser vertical resolution with 8 levels (respectively 18 levels) in the top 10 m (resp. 50 m). Such a configuration only enables to represent 70 % of the Dsst (Bernie et al., 2005). This could partly explain the underestimation of the Dsst in the model. Overestimated wind stress may also lead to an underestimation of the Dsst by inducing too strong vertical turbulent mixing and preventing from diurnal heating. In the Canary region, Dsst amplitudes are overestimated for the last quartile of amplitudes. As the model is warmer than SST data all over the year in this region (Fig. 14), these discrepancies may be due to local errors in surface heat fluxes. Elsewhere, the model distribution of Dsst amplitudes is in good agreement with data.

**NEMO on the shelf:
assessment of the
Iberia–Biscay–Ireland
configuration**C. Maraldi et al.

[Title Page](#)[Abstract](#)[Introduction](#)[Conclusions](#)[References](#)[Tables](#)[Figures](#)[⏪](#)[⏩](#)[◀](#)[▶](#)[Back](#)[Close](#)[Full Screen / Esc](#)[Printer-friendly Version](#)[Interactive Discussion](#)

to investigate the capability of the model to reproduce tidal surface ellipses in a region characterized by intense tidal currents.

6.1.3 FES2004

We use the last release of the Finite Element Solution (FES), called FES2004, for comparisons of barotropic tidal elevations (Lyard et al., 2006). The FES2004 tidal atlas is computed from the tidal hydrodynamic equations and tide gauge and satellite data assimilation. It has a global coverage and has been regridded onto a regular grid with a $1/8^\circ$ resolution. It is very accurate in the open ocean but larger errors can occur in shelf regions in coastal areas with complex shorelines. Thus, in addition to tide gauges, the FES2004 solution is useful tool to assess the modelled barotropic tidal solutions in the open ocean.

6.1.4 Altimetric data

We use 10 yr of TOPEX/Poseidon data combined with 7 yr of Jason-1 altimeter data spanning the period from September 1992 to January 2009 for the estimate of the internal tides signature in sea surface elevation. Altimetric data are not used for the validation of barotropic tides, as barotropic tides are compared to the FES2004 solution which assimilates altimetric data. The fraction of internal tides which is phase-locked with astronomical potential has sufficient coherence in both space and time for its surface signal to be detected in altimetric multi year time series (Ray and Mitchum, 1997). Along track sea surface heights have been extracted using the X-Track data processing tool (Lyard, 2008; Roblou et al., 2010). Data have been previously corrected from the barotropic response of the ocean to high-frequency atmospheric pressure and wind forcing (Carrère et Lyard, 2003) but no ocean tidal corrections were made. Along track harmonic analysis was performed to estimate the M_2 components which are used to study the time coherent internal tide signal.

NEMO on the shelf: assessment of the Iberia–Biscay–Ireland configuration

C. Maraldi et al.

Title Page

Abstract

Introduction

Conclusions

References

Tables

Figures

⏪

⏩

◀

▶

Back

Close

Full Screen / Esc

Printer-friendly Version

Interactive Discussion



6.2 Tidal elevations

The amplitudes and phases of the tidal constituents are derived from an harmonic analysis performed over the hourly modelled elevations of the ‘tide only’ run (run_{bt}, see Sect. 2.4) Comparisons between the model and the sea level observations at the tide gauge locations are made for the four principal tidal constituents (M_2 , S_2 , K_1 , O_1) and for the M_4 compound tidal constituent which is a non linear wave resulting from the interaction of M_2 with itself. The M_4 wave has negligible contribution in the open ocean but it is studied as it can reach large amplitudes on the European Shelf and especially in the English Channel (Le Provost and Fornerino, 1985). For each tidal constituent we have computed the RMS of the complex difference amplitude over the whole domain and over specific areas (Table 3). Errors are larger for the M_2 constituent that is the main harmonic over the area; mean error of the complex amplitude difference is 21.6 cm. Errors are not evenly distributed over the region. Mean error is lower than 3.3 cm around the Canary Islands, in the Mediterranean Sea and off West Iberia. Discrepancies between the model and the data are larger over extensive shelf areas where the model overestimates tidal amplitudes by up to 18% (RMS error up to up to 23 cm in the Bay of Biscay, in the English Channel, in the Irish Sea and in the Baltic Sea). In shelf regions, accurate bathymetry is a critical aspect of modelling as it strongly impacts the tidal wave propagation and the tidal amplitudes. Despite of significant improvements in the new bathymetry accuracy, some uncertainties may remain in shallow water regions, in particular in estuaries and small bays where some tide gauges are located. The bottom friction coefficient is also an important parameter for the tidal solution quality. In shallow water areas the flow is much more dependent on bottom friction and bottom friction dissipation is particularly large over the European shelf (Sternberg, 1968; Davies and Aldridge, 1993; Le Provost and Lyard, 1997). We used a constant bottom friction coefficient while it is highly variable over the domain due to the local nature of the seabed (Guillou and Chapalaina, 2010). This can yield inaccurate tidal solution and might partly explain local discrepancies in the English Channel

NEMO on the shelf: assessment of the Iberia–Biscay–Ireland configuration

C. Maraldi et al.

Title Page

Abstract

Introduction

Conclusions

References

Tables

Figures



Back

Close

Full Screen / Esc

Printer-friendly Version

Interactive Discussion



and also in the North Sea. Overestimated tidal elevations could also be explained by the absence of internal wave dissipation in the model physics.

Weaker errors are obtained for the other tidal components which have smaller tidal amplitudes. However large RMS errors are found for the M_4 component in the English Channel, the Irish Sea and the North Sea where M_4 amplitudes are larger.

The M_2 cotidal charts and their differences with the FES2004 solution are represented in Fig. 18. The IBI solution is in good agreement with FES2004 almost everywhere. Larger differences in amplitudes are found in the English Channel where amplitudes reach up to 3 m. Differences are found in the Alboran Sea where the IBI M_2 amplitudes are generally smaller than 10 cm. The western part of the Mediterranean basin is characterized by an amphidrome whose location is too far from the Spanish coast in comparison with the FES2004 solution and the solution of Tsimplis et al. (1995). In the Mediterranean Sea, the astronomical potential is very weak and full integral formulation (astronomical plus loading self/attraction potential) is needed to accurately model the tidal propagation (Ray, 1998). The model is only forced with the astronomical potential which could explain the discrepancies in the Mediterranean Sea. Further north, The M_2 cotidal charts are also in agreement with FES2004: amphidrome systems are very similar with slightly shifted positions in the IBI model east of England, between Northern Ireland and Scotland and along the southern coast of Norway.

6.2.1 Barotropic tidal currents

For barotropic current validation, comparisons between observed and modelled tidal ellipses from run_{bt} have been done for M_2 which is the most energetic tidal constituent in the region. Results are presented in Table 4 and Fig. 19 for bathymetry deeper than 50 m. Globally, the model shows good agreement with the observations and the RMS of the model-data misfits is 4.4 cm s^{-1} for the M_2 current amplitudes. The ellipse velocities tend to be overestimated by up to 35 % on the shelf areas as the Armorican and Celtic shelves (RMS of 4.1 cm s^{-1}) and in the Irish Sea (RMS of 5.3 cm s^{-1}) where the

NEMO on the shelf: assessment of the Iberia–Biscay–Ireland configuration

C. Maraldi et al.

Title Page

Abstract

Introduction

Conclusions

References

Tables

Figures

◀

▶

◀

▶

Back

Close

Full Screen / Esc

Printer-friendly Version

Interactive Discussion



has been performed, that is December 2007–January 2009 for the Donostia current time series and April 2008–February 2009 for the Matxitxako time series. Thus errors in the Donostia and Matxitxako modelled ellipses may be due to freshwater discharges that are not included in the model and may affect the tidal currents in surface. Below this layer (upper 30 m) the modelled profile is in good agreement with observations for the two current profiles (see Fig. 21 for the Matxitxako station). In the Gulf of Cadiz and in the Canary Island region, the modelled tidal currents are in good agreement with observations.

6.4 Internal tides

We used sea surface height data from altimetry to examine the M_2 internal tide signal in the Bay of Biscay. We consider the track TOPEX/Poseidon/Jason1 137 that crosses the Armorican shelf slope at nearly right angle (Fig. 1) as we expect the M_2 internal tides to propagate almost in the same direction. The method used to separate the barotropic tides from the time coherent internal tide signal consists in spatial filtering of the M_2 real and imaginary parts to remove the barotropic large scale signal (Ray and Mitchum, 1997). According to Pairaud et al. (2010) the wavelength of baroclinic mode 1 and mode 2 are, respectively 141 km and 75 km in the abyssal plain. Note that these values have been obtained using data collected during September-October 1994 and may vary with the stratification. To take into account the angle between the altimeter track and the internal tide direction of propagation we use a spatial cut-off slightly larger than the wavelength. We also filter at shorter scales to reduce the altimeter noise. Finally along track tidal components are filtered between 140 km and 210 km for mode 1 and between 60 km and 110 km for mode 2. The “residual tides” are obtained by removing the filtered signal to the harmonic components. Figure 22 presents the along track amplitudes and phase as computed from the altimetric data and from the model for mode 1 and for mode 2. It also presents the along track bathymetry. Indications attesting that the small oscillations are internal tides are: 1) oscillations are generated in the Armorican shelf slope region (45.8°N–46.0°N), 2) south of the shelf break the

NEMO on the shelf: assessment of the Iberia–Biscay–Ireland configuration

C. Maraldi et al.

Title Page

Abstract

Introduction

Conclusions

References

Tables

Figures



Back

Close

Full Screen / Esc

Printer-friendly Version

Interactive Discussion



phase increases constantly in the Bay of Biscay which indicates that the wave propagates away from the shelf, 3) for mode 1 and mode 2 we find wavelengths of approximately $(\lambda_1, \lambda_2) = (197 \text{ km}, 76 \text{ km})$ for the altimetric data and the model; these values are slightly larger but in good agreement with theoretical values. The overestimation may be due to a different stratification with the period studied in Pairaud et al. (2010) and to the angle between the satellite track and the across slope direction. Even if the model shows similar wavelengths than altimetric data we observe minor discrepancies in the baroclinic amplitudes and phases. For mode 1 (mode 2) there is a southward (northward) shift of the model sea surface signal. This may be the consequence of a different generation site in the model due to errors in the Armorican shelf slope representation. For the two modes model amplitudes are slightly overestimated especially near the generation site for mode 2. Both model and data indicate that the first mode has not the dominant surface signature in the Bay of Biscay.

7 A focus over the circulation on the European sea shelves

7.1 A focus on tidal fronts

While metrics have been defined and used to assess the model performances, in this section we evaluate the ability of the model to reproduce specific physics of the European shelf seas using qualitative comparisons. The occurrence of thermal fronts due to tidal mixing is a common feature on the European continental shelf. Thermal fronts appear in summer when most of the regions are dominated by thermal stratification. They separate tidally mixed waters from stratified waters. Two processes are involved in the tidal mixing of the water column: mixing associated with internal tides over shelf breaks which induce vertical motion of the seasonal thermocline and consequently induce a cooling of the mixed layer, and mixing through bottom friction in shallow water areas associated with strong tidal currents which tends to homogenize the water column and prevents from the formation of seasonal stratification. The MODIS SST data

NEMO on the shelf: assessment of the Iberia–Biscay–Ireland configuration

C. Maraldi et al.

Title Page

Abstract

Introduction

Conclusions

References

Tables

Figures

⏪

⏩

◀

▶

Back

Close

Full Screen / Esc

Printer-friendly Version

Interactive Discussion



NEMO on the shelf: assessment of the Iberia–Biscay–Ireland configuration

C. Maraldi et al.

Title Page

Abstract

Introduction

Conclusions

References

Tables

Figures



Back

Close

Full Screen / Esc

Printer-friendly Version

Interactive Discussion



with weaker tidal currents. The simulated temperature section exhibits a similar pattern. The mixed layer depth in the stratified waters is in good agreement with observations but the model is slightly colder by $\sim 0.3^\circ\text{C}$ below the MLD. The relaxing isopycnal slope between stratified and well mixed water is in good agreement with data. In the frontal region the model well represent the non coincidence between surface and bottom front positions. However the vertical resolution and the $1/36^\circ$ horizontal resolution are still not sufficient to correctly represent small structures in frontal and transition regions. The position of the front is relatively well reproduced in the model. Small differences in the frontal position may be due to tides. As the Ushant front is tidally induced it is very sensitive to the water column depth. In the mixed region the model bathymetry is about 20 m deeper than in the observations which may induce discrepancies in the frontal position. In this region, the temperature is more mixed in the model. As the MLD is relatively accurate in the stratified region, one can suppose that the bottom mixed layer is overestimated and reaches the MLD which induces a vertical mixing over the whole water column in the model. East of the internal front, data indicate thermal stratification while the model is well mixed. Between 5.05°W and 5°W , there is also a warmer layer in the upper 15 m in the data which is not modelled. This may be explained by local circulation: East of the transect very strong tidal currents are due to the presence of the island of Sein (48.0°N , 4.8°W). The model grid resolution is not sufficient to represent the island of Sein and the associated tidal currents are not modelled. In spite of some misfits, the model simulates well most of the dynamical aspects in the Ushant front region.

7.2 A focus on the circulation in the Southern Bay of Biscay

The analysis of the modelled SST and sea surface salinity (SSS) in the Bay of Biscay shows a warm and salty current flowing poleward along the Western and the Northern Iberian Peninsula and reaching the SW of France during winter 2007–2008 (Figs. 15 and 25, SSS not shown). The extension of the IPC at or near surface along the

provide a driving mechanism of the poleward current. When the current has reached Cap Finistere and turns eastward, its poleward flow is maintained by positive τ_x .

8 Conclusions

The aim of this study was 1) the definition of metrics for regional coastal simulations and 2) the assessment of the NEMO model on the IBI region using these metrics. It has been carried out for an hindcast simulation in 2008. Comparisons with the climatology, transport estimations, in situ and satellite data have been performed to assess the model performance.

The main contribution of the study was the definition of new metrics to validate the new model improvements which include the resolution of high frequency dynamics such as tides, the diurnal cycle and surges. A common methodology for validation procedures based on a validation plan and metrics implementation has been built. The procedure includes metrics developed within the MERSEA project for the verification of the model consistency, quality and performances in the deep ocean. It also includes complementary metrics upgraded for shelf and coastal regions. In particular, the contribution of the high-frequency and low-frequency dynamics has been investigated separately for EKE, SSH, currents and SST. Self-consistency metrics have also been used to evaluate the ability of the model to reproduce specific physics of the IBI region such as tidal front extensions and the Navidad SST signature. The validation exercise of the procedure has been tested during the MyOcean project. It has allowed a synthetic and complete assessment of the IBI configuration. The new metrics developed within this work could be used for other regional model assessment. Besides, the procedure defined in this article will serve as a basis for the IBI real-time validation and could also be used for defining Cal/Val strategies in an operational context for other regional forecast systems. From this extensive scientific assessment, a procedure has already been derived to assess the necessary improvements between versions of the MyOcean IBI system based on Taylor diagrams. A subsample of these metrics was

NEMO on the shelf: assessment of the Iberia–Biscay–Ireland configuration

C. Maraldi et al.

Title Page

Abstract

Introduction

Conclusions

References

Tables

Figures

⏪

⏩

◀

▶

Back

Close

Full Screen / Esc

Printer-friendly Version

Interactive Discussion



chosen based on the availability of observations in real time or near real time. This sub sample (mainly a check of T, S profiles, AVISO SLA, OSTIA SST, and moorings time series) is currently used to control the quality of the IBI forecast in real time and in quarterly reports in partnership with the global Monitoring & Forecasting Centers (Lellouche et al., this issue).

We have shown that the general circulation in the IBI area is well modelled and mass fluxes are in good agreement with previous estimates computed from observations. However differences are found for the representation of the Mediterranean water which is too light in the model. The discrepancies are mainly due to the initial conditions extracted from the PSY2V3 model. The model SST is globally well modelled and stays within the range of satellite data precision. Major discrepancies appear in upwelling regions where the model SST is too cold. This may be partly due to the wind stress forcing fields which are too strong in comparison with in situ measurements. Errors in forcing wind stress also induce overestimated residual currents and underestimated SST diurnal cycle in comparison with buoy observations. Comparisons with in situ profiles have shown that the MLD is underestimated in winter which is linked to a too small wave-induced mixing during months with weak wind stress. Comparisons with tidal elevations and tidal currents have shown that tides are accurately modelled and that the main discrepancies are likely to be explained by errors in the bathymetry. Qualitative comparisons with SST data have shown that the model represents well tidal fronts over the European shelf. The last section dedicated to the study of the Navidad event of winter 2007–2008 has shown the ability of the model to represent coastal processes specific of the IBI area. However more data would be required to verify whether the modelled intensity of this event is realistic or not.

The PSY2V3 solution has been recently improved. In particular the MW core is now in better agreement with climatology (MW core at ~ 1200 m in PSY2). Initialization and open boundary fields taken from this new simulation should improve the MW representation in the IBI solution. MLD discrepancies should be improved with a more realistic wave-induced parameterization or with a wave model coupling. Tidal solutions may

**NEMO on the shelf:
assessment of the
Iberia–Biscay–Ireland
configuration**

C. Maraldi et al.

Title Page

Abstract

Introduction

Conclusions

References

Tables

Figures



Back

Close

Full Screen / Esc

Printer-friendly Version

Interactive Discussion



also be improved by further improvements in the bathymetry and further tuning in the bottom friction as a spatial dependence with the seabed nature. This study was a first step towards the setup of an operational ocean forcing system in the IBI area. We have characterized the model uncertainties to highlight elements that will need future model developments. Data assimilation will be the next step to improve the simulation. Further work on model assessment should also rely on altimetric data. In particular, we plan to explore metrics that would allow us to characterize the mesoscale and sub-mesoscale activity in the simulation.

Acknowledgements. This research was supported by the MyOcean European project through its partnership with CNRS (Centre National de la Recherche Scientifique). The authors gratefully acknowledge the receipt of buoy and tide gauge data from Puertos del Estado, of buoy data from Météo France, the Marine Institute and the AZTI, of tide gauge and along track altimetric data from Collecte Localisation Satellites, of radar HF data provided by Fabrice Ardhuin and SHOM, of historical current meter data from BODC, of CTD data collected during the MOUTON campaign and provided by SHOM. We thank the Mercator Ocean teams, Charly Reignier and Clément Bricaud whose hard work made this study possible. This study benefited from fruitful discussions with Gildas Cambon concerning the Ushant thermal front.



The publication of this article is financed by CNRS-INSU.

OSD

9, 499–583, 2012

NEMO on the shelf: assessment of the Iberia–Biscay–Ireland configuration

C. Maraldi et al.

Title Page

Abstract

Introduction

Conclusions

References

Tables

Figures

⏪

⏩

◀

▶

Back

Close

Full Screen / Esc

Printer-friendly Version

Interactive Discussion



References

- Alvarez, M., Perez, F. F., Bryden, H. L., and Rios, A. F.: Physical and biochemical transports structure in the North Atlantic subpolar gyre, *J. Geophys. Res.*, 109, C03027, doi:10.1029/2003JC002015, 2004.
- 5 André, G., Garreau, P., and Fraunie, P.: Mesoscale slope current variability in the Gulf of Lions. Interpretation of in-situ measurements using a three dimensional model, *Cont. Shelf Res.*, 29, 407–423, 2009.
- Andersson, L. and Rydberg, L.: Exchange of water and nutrients between the Skagerrak and the Kattegat, *Estuar. Coast. Shelf S.*, 36 (2), 159–181, 1993.
- 10 Astraldi, M. and Gasparini, G. P.: The seasonal characteristics of the circulation in the North Mediterranean Basin and their relationship with the atmospheric-climatic conditions, *J. Geophys. Res.*, 97 (C6), 9531–9540, doi:10.1029/92JC00114, 1992.
- Barnier, B., Madec, G., Penduff, T., Molines, J.-M., Treguier, A.-M., Le Sommer, J., Beckmann, A., Biastoch, A., Böning, C., Dengg, J., Derval, C., Durand, E., Gulev, S., Remy, E., Talandier, C., Theetten, S., Maltrud, M., McClean, J., and De Cuevas, B.: Impact of partial steps and momentum advection schemes in a global ocean circulation model at eddy-permitting resolution. *Ocean Dynam.*, 56, 543–567, doi:10.1007/s10236-006-0082-1, 2006.
- 15 Barth, A., Alvera-Azcarate, A., Rixen, M., and Beckers, J.-M.: Two-way nested model of mesoscale circulation features in the Ligurian Sea, *Prog. Oceanogr.*, 66, 171–189, 2005.
- 20 Becker, J. J., Sandwell, D. T., Smith, W. H. F., Braud, J., B. Binder, B., Depner, J., Fabre, D., Factor, J., Ingalls, S., Kim, S.-H., Ladner, R., Marks, K., Nelson, S., Pharaoh, A., Trimmer, R., Von Rosenberg, J., Wallace, G., and Weatherall, P.: Global bathymetry and elevation data at 30 arc seconds resolution: SRTM30_PLUS, *Mar Geod.*, 32 (4), 355–371, 2009.
- Benzhora, M. and Millot, C.: Characteristics and circulation of the surface and intermediate water masses off Algeria, *Deep-Sea Res.*, 42 (10), 1803–1830, 1995.
- 25 Bernie, D. J., Woolnough, S. J., Slingo, J. M., and Guilyardi, E.: Modelling diurnal and intraseasonal variability of the ocean mixed layer, *J. Climate*, 18 (8), 1190–1202, 2005.
- Béthoux, J. P.: Mean water fluxes across sections in the Mediterranean Sea, evaluated on the basis of water and salt budgets and observed salinities, *Oceanol. Acta*, 3, 79–88, 1980.
- 30 Béthoux, J. P., Prieur, L., and Nyffeler, F.: The water circulation in the North-Western Mediterranean Sea; its relations with wind and atmospheric pressure, *Hydrodynamics of Semi-Enclosed Seas: Proceedings of the 13th International Liege Colloquium on Ocean*

NEMO on the shelf: assessment of the Iberia–Biscay–Ireland configuration

C. Maraldi et al.

Title Page

Abstract

Introduction

Conclusions

References

Tables

Figures

⏪

⏩

◀

▶

Back

Close

Full Screen / Esc

Printer-friendly Version

Interactive Discussion



NEMO on the shelf: assessment of the Iberia–Biscay–Ireland configuration

C. Maraldi et al.

Title Page

Abstract

Introduction

Conclusions

References

Tables

Figures

⏪

⏩

◀

▶

Back

Close

Full Screen / Esc

Printer-friendly Version

Interactive Discussion



Hydrodynamics, edited by: Nihoul, J. C. J., Elsevier, 34, 129–142, doi:10.1016/S0422-9894(08)71240-6, 1982.

Blayo, E. and Debreu, L.: Revisiting open boundary conditions from the point of view characteristic variables, *Ocean Model.*, 9, 231–253, 2005.

5 Bowers, D. G. and Simpson, J. H.: Mean positions of tidal fronts in European Shelf Sea, *Cont. Shelf Res.*, 7, 35–44, 1987.

Boyer, T. P., Antonov, J. I., Baranova, O. K., Garcia, H., Johnson, D. R., Locarnini, R. A., Mishonov, A. V., Pitcher, M. T., and Smolyar, I.: *World Ocean Database 2005*. NOAA Atlas NESDIS, edited by: Levitus, S., NOAA, Silver Spring, 60, 182 pp., 2006.

10 Brown, J. and Gmitrowitz, E. M.: Observations of the transverse structure and dynamics of the low frequency flow through the North Channel of the Irish Sea, *Cont. Shelf Res.*, 15 (9), 1133–1156, 1995.

Brown, J., Carrillo, L., Fernanda, L., Horsburgh, K. J., Hill, A. E., Young, E. F., and Medler, K. J.: Observations of the physical structure and seasonal jet-like circulation of the Celtic Sea and St. George's Channel of the Irish Sea, *Cont. Shelf Res.*, 23 (6), 533–561, 2003.

15 Candela, J., Winant, C., and Ruiz, A.: Tides in the Strait of Gibraltar, *J. Geophys. Res.*, 95 (C5), 7313–7335, 1990.

Carrère, L. and Lyard, F.: Modelling the barotropic response of the global ocean to atmospheric wind and pressure forcing – comparisons with observations, *Geophys. Res. Lett.*, 30, 6, 2003.

20 Chelton, D. B. and Schlax, M. G.: Global observations of oceanic Rossby waves, *Science*, 272, 264–238, 1996.

Coelho, H. S., Neves, R. J. J., White, M., Leitao, P. C., and Santos, A. J.: A model for ocean circulation on the Iberian coast, *J. Marine Syst.*, 32, 153–179, 2002.

25 Davies, A. M. and Aldridge, J. N.: A numerical model study of parameters influencing tidal currents in the Irish Sea, *J. Geophys. Res.*, 98 (C4), 7049–7067, 1993.

Davies, A. M., Kwong, S. C. M., and Flather, R. A.: A three-dimensional model of diurnal and semidiurnal tides on the European shelf, *J. Geophys. Res.*, 102 (C4), 8625–8656, 1997.

30 Dréville, M., Bourdallé-Badie, R., Derval, C., Drillet, Y., Lellouche, J.-M., Rémy, E., Tranchant, B., Benkiran, M., Greiner, E., Guinehut, S., Verbrugge, N., Garric, G., Testut, C.-E., Laborie, M., Nouel, L., Bahurel, P., Bricaud, C., Crosnier, L., Dombrowsky, E., Durand, E., Ferry, N., Hernandez, F., Galloudec, O., Messal, F., and Parent, L.: The GO-DAE Mercator-Océan global ocean forecasting system: results, applications and prospects,

NEMO on the shelf: assessment of the Iberia–Biscay–Ireland configuration

C. Maraldi et al.

Title Page

Abstract

Introduction

Conclusions

References

Tables

Figures

◀

▶

◀

▶

Back

Close

Full Screen / Esc

Printer-friendly Version

Interactive Discussion

doi:10.1016/j.csr.2010.01.018, 2010.

Hansen, B. and Østerhus, S.: North Atlantic–Nordic Seas exchanges, *Prog. Oceanogr.*, 45, 109–208, 2000.

Hansen, B., Malmberg, S. A., Saelen, O. H., and Østerhus, S.: Measurements of flow north of the Faroe Islands June 1986, *ICES Coop. Res. Rep.*, 225, 83–95, 1998.

Hansen, B., Østerhus, S., Hatun, H., Kristiansen, R., and Larsen, K. M. H.: The Iceland–Faroe inflow of Atlantic water to the Nordic Seas, *Prog. Oceanogr.*, 59, 443–474, 2003.

Harvey, J. and Arhan, M.: The water masses of the Central North Atlantic in 1983–84, *J. Phys. Oceanogr.*, 18 (12), 1855–1875, 1988.

Herbert, G., Ayoub, N., Marsaleix, P., and Lyard, F.: Signature of the coastal circulation variability in altimetric data in the Southern Bay of Biscay during winter and fall 2004, *J. Marine Syst.*, 88 (2), 139–158, 2011.

Hernandez-Guerra, A., Machin, F., Antoranz, A., Cisneros-Aguirre, J., Gordo, C., Marrero-Diaz, A., Martinez, A., Ratsimandresy, A. W., Rodriguez-Santana, A., Sangra, P., Lopez-Laazen, F., Parilla, G., and Pelegri, J. L.: Temporal variability of mass transport in the Canary Current, *Deep-Sea Res.*, 49, 3415–3426, 2002.

Herrmann, M., Estournel, C., Déqué, M., Marsaleix, P., Sevaut, F., and Somot, S.: Dense water formation in the Gulf of Lions shelf: impact of atmospheric interannual variability and climate change, *Cont. Shelf Res.*, 28, 2092–2112 doi:10.1016/j.csr.2008.03.003, 2008.

Holliday, N. P., Pollard, R. T., Read, J. F., and Leach, H.: Water mass properties and fluxes in the Rockall Trough, 1975–1998, *Deep-Sea Res Pt. I*, 47, 1303–1332, 2000.

Holt, J. T., James, I. D., and Jones, J. E.: An s coordinate density evolving model of the North-west European continental shelf – 2, seasonal currents and tides, *J. Geophys. Res.*, 106 (C7), 14035–14053, 2001.

Holt, J. and Umlauf, L.: Modelling the tidal mixing fronts and seasonal stratification on the Northwest European shelf, *Cont. Shelf Res.*, 28, 887–903, 2008.

Howarth, M. J.: Non-tidal flow in the North Channel of the Irish Sea. *Hydrodynamics of Semi-Enclosed Seas: Proceedings of the 13th International Liege Colloquium on Ocean Hydrodynamics*, edited by: Nihoul, J. C. J., Elsevier, 205–241, 1982.

Howe, M. R.: Current and hydrological measurements in the Mediterranean Undercurrent near Cape St. Vincent, *Oceanol. Acta*, 7 (2), 163–168, 1984.

Ingleby, B. and Huddleston, M.: Quality control of ocean temperature and salinity profiles–historical and real time data, *J. Marine Syst.*, 65, 158–175, 2007.

NEMO on the shelf: assessment of the Iberia–Biscay–Ireland configuration

C. Maraldi et al.

Title Page

Abstract

Introduction

Conclusions

References

Tables

Figures

⏪

⏩

◀

▶

Back

Close

Full Screen / Esc

Printer-friendly Version

Interactive Discussion



- Jorge da Silva, A.: The slope current off the West Iberian coast in autumn, ICES C. M., 1996, 35, 1996.
- Juza, M.: Collocation and validation tools for the DRAKKAR ensemble of simulations. Technical report, MEOM-LEGI, Grenoble, France, 2008.
- 5 Krauss, W.: Currents and mixing in the Irminger Sea and in the Iceland Basin, J. Geophys. Res., 100 (C6), 10,851–10,871, 1995.
- Lafuente, J. G., Delgado, J., Vargas, J. M., Vargas, M., Plaza, F., and Sarhan, T.: Low-frequency variability of the exchanged flows through the Strait of Gibraltar during CANIGO, Deep-Sea Res. Pt. II, 49, 4051–4067, 2002.
- 10 Large, W. G. and Yeager S. G.: Diurnal to decadal global forcing for ocean and sea-ice models: the data sets and flux climatologies. NCAR Technical Note: NCAR/TN-460+STR. CGD Division of the National Center for Atmospheric Research, 2004.
- Le Borgne, P., Marsouin, A., Orain, F., and Roquet, H.: Operational sea surface temperature bias adjustment using AATSR data, Remote Sens. Environ., 116, 93–106, 2011.
- 15 Le Boyer, A., Cambon, G., Daniault, N., Herbette, S., Le Cann, B., Marié, L., and Morin, P.: Observations of the Ushant tidal front in September 2007, Cont. Shelf Res., 29 (8), 1026–1037, 2009.
- Le Cann, B. and Serpette, A.: Intense warm and saline upper ocean inflow in the Southern Bay of Biscay in autumn-winter 2006–2007, Cont. Shelf Res., 29, 1014–1025, 2009.
- 20 Le Hénaff, M., De Mey, P., and Marsaleix, P.: Assessment of observational networks with the Representer Matrix Spectra method-application to a 3-D coastal model of the Bay of Biscay, Ocean Dynam., 59, 3–20 doi:10.1007/s10236-008-0144-7, 2009.
- Lellouche, J.-M., Le Galloudec, O., Drévilion, M., Régnier, C., Desportes, C., Tranchant, B., Testut, C.-E., Greiner, E., Garric, G., Bourdallé-Badie, R., Bricaud, C., Ferry, N., Drillet, Y., Daudin, A., and De Nicola, C.: Overview and scientific assessment of the MyOcean/Mercator Océan global ocean monitoring and forecasting system, Ocean Sci. Discuss., in preparation, 25 2012.
- Le Provost, C. and Fornerino, M.: Tidal spectroscopy of the English Channel with a numerical model, J. Phys. Oceanogr., 15, 1009–1031, 1985.
- 30 Le Provost, C. and Lyard, F.: Energetics of the M_2 barotropic ocean tides: an estimate of bottom friction dissipation from a hydrodynamic model, Prog. Oceanogr., 40, 37–52, 1997.
- Le Provost, C., Bell, M.J., Greiner, E., McCulloch, P., and De Mey, P.: GODAE Internal Metrics for model performance evaluation and intercomparison, CNRS/LEGOS, Ed., Toulouse,

NEMO on the shelf: assessment of the Iberia–Biscay–Ireland configuration

C. Maraldi et al.

Title Page

Abstract

Introduction

Conclusions

References

Tables

Figures

⏪

⏩

◀

▶

Back

Close

Full Screen / Esc

Printer-friendly Version

Interactive Discussion



France, 2001.

Lherminier, P., Mercier, H., Gourcuff, C., Alvarez, M., Bacon, S., and Kermabon, C.: Transports across the 2002 Greenland–Portugal Ovide section and comparison with 1997, *J. Geophys. Res.*, 112, C07003, doi:10.1029/2006JC003716, 2007.

5 Llope, M., Anadon, R., Viesca, L., Quevedo, M., Gonzalez-Quiros, R., and Stenseth, N. C.: Hydrography of the Southern Bay of Biscay shelf-break region: integrating the multi-scale physical variability over the period 1993–2003, *J. Geophys. Res.*, 111 (C09021), doi:10.1029/2005JC002963, 2006.

Lyard, F.: Les processus rapides de la dynamique océanique observation et modélisation
10 Mémoire d’habilitation à diriger les recherches, Université de Toulouse, Toulouse, France, 2006.

Lyard, F., Lefevre, F., Letellier, T., and Francis, O.: Modelling the global ocean tides: modern insights from FES2004, *Ocean Dynam.*, 56, 394–415, 2006.

Machin, F. and Pelegri, J. L.: Effect of the Canary Islands in the blockage and mixing of the North Atlantic eastern water masses, *Geophys. Res. Lett.*, 33, L04605, doi:10.1029/2005GL025048, 2006.

Machin, F., Hernandez-Guerra, A., and Pelegri, J. L.: Mass fluxes in the Canary Basin, *Prog. Oceanogr.*, 70, 416–447, 2006.

Madec, G.: NEMO Ocean General Circulation Model Reference Manuel, Internal Report, LODYC/IPSL, Paris, 2008.

Madec, G., Delecluse, P., Imbard, M., and Lévy, C.: OPA 8.1 Ocean general circulation model reference manual. Institut Pierre-Simon Laplace, Paris, France, 20, 91, 1998.

Mariette, V. and Le Cann, B.: Simulation of the formation of Ushant thermal front, *Cont. Shelf Res.*, 4 (6), 637–660, 1985.

25 Mauritzen, C., Morel, Y., and Paillet, J.: On the influence of Mediterranean water on the central waters of the North Atlantic Ocean, *Deep-Sea Res. Pt. I*, 48, 347–381, 2001.

Mazé, J. P., Arhan, M., and Mercier, H.: Volume budget of the eastern boundary layer off the Iberian Peninsula, *Deep-Sea Res. Pt. I*, 44 (9–10), 1543–1574, 1997.

Morel, A., Huot, Y., Gentili, B., Werdell, P. J., Hooker, S. B., and Franz, B. A.: Examining the consistency of products derived from various ocean color sensors in open ocean (Case 1)
30 waters in the perspective of a multi-sensor approach, *Remote Sens. Environ.*, 111 (1), 69–88, 2007.

Muller, H., Blanke, B., Dumas, F., Lekien, F., and Mariette, V.: Estimating the Lagrangian resid-

NEMO on the shelf: assessment of the Iberia–Biscay–Ireland configuration

C. Maraldi et al.

Title Page

Abstract

Introduction

Conclusions

References

Tables

Figures

⏪

⏩

◀

▶

Back

Close

Full Screen / Esc

Printer-friendly Version

Interactive Discussion



- ual circulation in the Iroise Sea, *J. Marine Syst.*, 78 (1), S17–S36, 2009.
- Onken, R., Robinson, A. R., Lermusiaux, P. F. J., Haley, P. J., and Anderson, L. A.: Data-driven simulations of synoptic circulation and transports in the Tunisia–Sardinia–Sicily region, *J. Geophys. Res.*, 108 (C9), 8123, doi:10.1029-2002JC001348, 2003.
- 5 Østerhus, S., Turrell, W. R., Jonsson, S., and Hansen, B.: Measured volume, heat, and salt fluxes from the Atlantic to the Arctic Mediterranean, *Geophys. Res. Lett.*, 32, doi:10.1029/2004GL022188, 2005.
- Otto, L., Zimmerman, J. T. F., Furnes, G. K., Mork, M., Saetre, R., and Becker, G.: Review of the physical oceanography of the North Sea, Netherlands, *J. Sea Res.*, 26, 161–238, 1990.
- 10 Pairaud, I., Auclair, F., Marsaleix, P., Lyard, F., and Pichon, A.: Dynamics of the semi-diurnal and quarter-diurnal tides in the Bay of Biscay. Part 2: Baroclinic tides, *Cont. Shelf Res.*, 30, 253–269, 2010.
- Peliz, A., Dubert, J., Marchesiello, P., and Tele-Macado, A.: Surface circulation in the Gulf of Cadiz: model and mean flow structure, *J. Geophys. Res.*, 112 (C11015), doi:10.1029/2007JC004159, 2007.
- 15 Peliz, A., Marchesiello, P., Santos, A. M. P., Dubert, J., Tele-Macado, A., Marta-Almeida, M., and Le Cann, B.: Surface circulation in the Gulf of Cadiz: 2. Inflow-Outflow coupling and the Gulf of Cadiz slope current, *J. Geophys. Res.*, 114 (C03011), doi:10.1029/2008JC004771, 2009.
- 20 Pichon, A. and Correard, S.: Internal tides modelling in the Bay of Biscay. Comparisons with observations, *Scientia Marina*, 70, 65–88, 2006.
- Pimentel, S., Haines, K., and Nichols, N. K.: Modeling the diurnal variability of sea surface temperatures, *J. Geophys. Res.*, 113, C11004, doi:10.1029/2007JC004607, 2008.
- Pingree, R. D. and Le Cann, B.: Structure, strength and seasonality of the slope currents in the Bay of Biscay region, *J. Mar. Biol. Assoc.UK*, 70, 857–885, doi:10.1017/S0025315400059117, 1990.
- 25 Pingree, R. D. and Le Cann, B.: Three anticyclonic Slope Water oceanic eDDIES (SWODDIES) in the Southern Bay of Biscay in 1990, *Deep-Sea Res.*, 39, 1147–1175, 1992.
- Pingree, R. D., Mardell, G. T., and New, A. L.: Propagation of internal tides from the upeer slopes of the Bay of Biscay, *Nature*, 321, 154–158, 1986.
- 30 Pinot, J.-M., Lopez-Jurado, J. L., and Riera, M.: The CANALES experiment (1990–1998). Interannual, seasonal, and mesoscale variability of the circulation in the Balearic Channels, *Prog. Oceanogr.*, 55, 335–370, 2002.

NEMO on the shelf: assessment of the Iberia–Biscay–Ireland configuration

C. Maraldi et al.

Title Page

Abstract

Introduction

Conclusions

References

Tables

Figures

⏪

⏩

◀

▶

Back

Close

Full Screen / Esc

Printer-friendly Version

Interactive Discussion



- Prandle, D., Ballard, G., Flatt, D., Harrison, A. J., Jones, S. E., Knight, P. J., Loch, S., McManus, J., Player, R., and Tappin, A.: Combining modelling and monitoring to determine fluxes of water, dissolved and particulate metals through the Dover Strait, *Cont. Shelf Res.*, 16 (2), 237–257, 1996.
- 5 Pujol, M.-I. and Larnicol, G.: Mediterranean sea eddy kinetic energy variability from 11 years of altimetric data, *J. Marine Syst.*, 58 (3–4), 121–142, 2002.
- Ray, R. D.: Ocean self-attraction and loading in numerical tidal models, *Mar. Geod.*, 21, 181–192, 1998.
- Ray, R. D. and Mitchum, G. T.: Surface manifestation of internal tides in the deep ocean: observation from altimetry and island gauges, *Prog. Oceanogr.*, 40, 135–162, 1997.
- 10 Reffray, G., Fraunié, P., and Marsaleix, P.: Secondary flows induced by wind forcing in the Rhône region of freshwater influence, *Ocean Dynam.*, 54, 179–196. doi:10.1007/s10236-003-0079-y, 2004.
- Rhein, M. and Hinrichsen, H. H.: Modification of Mediterranean water in the Gulf of Cadiz, studied with hydrographic, nutrient and chlorofluoromethane data, *Deep-Sea Res. Pt. I*, 40 (2), 267–291, 2003.
- Roblou, L., Lamouroux, J., Bouffard, J., Lyard, F., Le Hénaff, M., Lombard, A., Marsaleix, P., De Mey, P., and Birol, F.: Post-processing altimeter data toward coastal applications and integration into coastal models, in: *Coastal Altimetry*, edited by: Vignudelli, S., Kostianoy, A., and Cipollini, P., Benveniste, J., Springer, 2010.
- 20 Rodhe, J.: On the dynamics of the large-scale circulation of the Skagerrak, *J. Sea Res.*, 35 (1–3), 9–21, 1996.
- Rubio, A., Barnier, B., Jorda, G., Espino, M., and Marsaleix, P.: Origin and dynamics of mesoscale eddies in the Catalan Sea (NW Mediterranean): insight from a numerical model study, *J. Geophys. Res.*, 114, C06009, doi:10.1029/2007JC004245, 2009.
- 25 Rubio, A., Fontán, A., Lazure, P., González, M., Valencia, V., Ferrer, L., Mader, J., and Hernández, C.: On the seasonal variability of currents and temperature in waters of the continental slope, Southern Bay of Biscay, *J. Marine Syst.*, submitted, 2012.
- Rydberg, L., Hammer, J., and Liungman, O.: Fluxes of water and nutrients within and into the Skagerrak, *J. Sea Res.*, 35 (1–3), 23–28, 1996.
- 30 Sammari, C., Millot, C., and Prieur, L.: Aspects of the seasonal and mesoscale variabilities of the Northern Current in the Western Mediterranean Sea inferred from the PROLIG-2 and PROS-6 experiments, *Deep-Sea Res. Pt. I*, 42 (6), 893–917, 1995.

- ranean Sea, *J. Geophys. Res.*, 100 (C8), 16,223–16,239, 1995.
- Turrell, W. R., Hansen, B., Hughes, S., and Østerhus, S.: Hydrographic variability during the decade of the 1990s in the Northeast Atlantic and Southern Norwegian Sea, *ICES Mar. Sc.*, 219, 111–120, 2003.
- 5 Umlauf, L. and Burchard, H.: A generic length-scale equation for geophysical turbulence models, *J. Mar. Res.*, 61 (2), 235–265, 2002.
- Van Aken, H. M.: Surface currents in the Bay of Biscay observed with drifters between 1995 and 1999, *Deep-Sea Res.*, 49, 1071–1086, 2002.
- Van Aken, H. M. and Becker, G.: Hydrography and trough-flow in the North-Eastern North Atlantic Ocean: the NANSEN project, *Prog. Oceanogr.*, 38, 297–346, 1993.
- 10 Vélez-Belchí, P., Vargas-Yáñez, M. and Tintoré, J.: Observation of a Western Alborán Gyre migration event, *Prog. Oceanogr.*, 66, 190–210, 2005.
- Visser, A. W., Souza, A. J., Hessner, K., and Simpson, J. H.: The effect of stratification on tidal current profiles in a region of freshwater influence, *Oceanol. Acta*, 17 (4), 369–382, 1994.
- 15 Von Schuckmann, K., Gaillard, F., and Le Traon, P.-Y.: Global hydrographic variability patterns during 2003–2008, *J. Geophys. Res.*, 114, C09007, doi:10.1029/2008JC005237, 2009.
- White, M. and Bowyer, P.: The shelf-edge current north-west of Ireland, *Ann. Geophys.*, 15, 1076–1083, doi:10.1007/s00585-997-1076-0, 1997.
- 20 Wunsch, C. and Stammer, D.: Atmospheric loading and the oceanic “inverse barometer” effect, *Rev. Geophys.*, 35 (1), 79–107, 1997.

NEMO on the shelf: assessment of the Iberia–Biscay–Ireland configuration

C. Maraldi et al.

Title Page

Abstract

Introduction

Conclusions

References

Tables

Figures

◀

▶

◀

▶

Back

Close

Full Screen / Esc

Printer-friendly Version

Interactive Discussion



NEMO on the shelf: assessment of the Iberia–Biscay–Ireland configuration

C. Maraldi et al.

[Title Page](#)
[Abstract](#)
[Introduction](#)
[Conclusions](#)
[References](#)
[Tables](#)
[Figures](#)
[◀](#)
[▶](#)
[◀](#)
[▶](#)
[Back](#)
[Close](#)
[Full Screen / Esc](#)
[Printer-friendly Version](#)
[Interactive Discussion](#)

Table 1. List of in situ buoys used in this study. For each buoy, the longitude, latitude, and variable available at the station and the organism providing the data are indicated. The variables that may be available are: sea surface temperature (SST), sea surface salinity (SSS), currents (U,V) at the surface for Puertos del Estado buoys and in the first 200 m currents along the water column depth for AZTI buoys and atmospheric variables (AV) that include air temperature, atmospheric pressure and wind velocity.

Mooring name	Lon	Lat	SST	SSS	UV	AV	Organism
Cadiz_Buoy	-6.96	36.48	✓	✓	✓	✓	Puertos del Estado
Cabo Silleiro	-9.40	42.12	✓	✓	✓	✓	Puertos del Estado
Villano Sisargas	-9.21	43.49	✓	✓	✓	✓	Puertos del Estado
Estaca Bares	-7.62	44.06	✓	✓	✓	✓	Puertos del Estado
Cabo Penas	-6.17	43.73	✓	✓	✓	✓	Puertos del Estado
Sanatander	-3.77	43.84	✓	✓	✓	✓	Puertos del Estado
Bilao	-3.04	43.63	✓	✓	✓	✓	Puertos del Estado
Tenerife	-16.58	28.00	✓	✓	✓	✓	Puertos del Estado
Gran Canaria	-15.81	28.19	✓	✓	✓	✓	Puertos del Estado
M1	-11.20	53.13	✓				Marine institute
M2	-5.42	53.48	✓				Marine institute
M3	-10.55	51.22	✓				Marine institute
M4	-10.00	55.00	✓				Marine institute
M5	-6.70	51.69	✓				Marine institute
M6	-15.93	53.06	✓				Marine institute
Brittany	-8.50	47.50	✓				Météo France
Gascogne	-5.00	45.20	✓				Météo France
Lion	4.70	42.10	✓				Météo France
Ouessant	-5.75	48.50	✓				Météo France
Donostia	-2.02	43.56	✓	✓	✓		AZTI
Matxitxako	-2.69	43.63	✓	✓	✓		AZTI

NEMO on the shelf: assessment of the Iberia–Biscay–Ireland configuration

C. Maraldi et al.

Title Page

Abstract

Introduction

Conclusions

References

Tables

Figures



Back

Close

Full Screen / Esc

Printer-friendly Version

Interactive Discussion

Table 2a. Transport estimates from the model and the literature. Model transports are estimated from monthly fields and mean and RMS values are presented. Units are Sv. Values in green (resp. in red) indicate net northward transports (resp. net southward transports) or net eastward transports (net westward transports) for zonal sections as computed from observations. Values in black indicate net transports. Estimations in bold are used for Fig. 5.

	Ext. 1	Ext. 2	Transport classes	Model values Mean/StdDev	Published Estimations	References
Gibraltar	−5.74E 35.70N	−5.74° E 36.20° N	S < 37.25 S > 37.25	0.48/0.05 −0.49/0.5	0.66−0.97 −0.84−−0.57	Tsimplis and Bryden, 2000; Lafuente et al., 2002
Mallorca-Spain	3.10° E 39.80° N	2.00° E 41.40° N	NO	−091/0.55	1.5−−0.75	Béthoux, 1980; Font et al., 1988; Schroeder et al., 2008
Ibiza Channel	0.00° E 38.75° N	1.37° E 39.00° N	NO	0.65/0.27 −1.33/0.47	0.2−0.7 −1.6−−0.2	Béthoux, 1980; Font et al., 1988; Pinot et al., 2002
Sardinia Channel	9.00° E 36.80° N	9.00° E 39.37° N	S < 38.5 S > 38.5	1.24/0.58 −078/0.28	0.50−1.85 1.30−−0.20	Garzoli and Maillard, 1979; Béthoux, 1980; Sammari et al., 1999; Onken et al., 2002
North Corsica	7.20° E 43.70° N	8.75° E 42.50° N	0 < z < 200	0.90/0.12 −1.28/0.35	0.7 −1.5−−0.9	Béthoux, 1982; Astraldi and Gasparini, 1992; Sammari et al., 1995; Barth et al., 2005
			200 < z < 700	0.75/0.21 −0.80/0.22	0.2 −0.4−−0.2	
			0 < z < 700	1.65/0.27 −2.07/0.52	0.9−1.15 −1.9−−1.0	
Gulf Lion	5.12° E 42.50° N	5.12° E 43.40° N	0 < z < 500	−1.51/0.44	1.18	André et al., 2009
Cadiz Gulf	−8.50° E 32.00° N	−8.50° E 38.20° N	$\sigma_1 < 31.7$ 31.7 < σ_1	1.77/0.24 −0.04/0.16	3.1 −2.8	Mauritzen et al., 2001
North Cadiz Gulf	−8.50° E 35.40° N	−8.50° E 38.20° N	32.0 < σ_1 < 36.8	−0.74/1.07	−6.5−−2.7	Howe, 1984; Rhein and Hinrichsen, 1993; Mauritzen et al., 2001
Azores Current	−14.00° E 33.00° N	−14.00° E 37.00° N	z < 1500	15.10/4.53 −12.25/6.17	13.7 −4.7	Peliz et al., 2007
Algerian Current	2.00° E 36.50° N	2.00° E 38.00° N	$\sigma < 29.0$ 29.0 < σ < 33.465 33.465 < σ	0.63/0.50 0.58/0.45 1.01/0.56	1.07−2.26 0.02−0.20 −0.16	Béthoux, 1980; Benzhora and Millot, 1995; Schroeder et al., 2008
Lanzarote-Africa	−11.10° E 28.70° N	−13.90° E 28.70° N	$\sigma < 27.3$ 27.3 < σ < 7.7	−0.41/1.14 0.02/0.42	−2.50−−0.60 0.1	Hernandez-Guerra et al., 2002; Machin and Pelegrí, 2006; Machin et al., 2006
Fuerteventura-Gran Canaria	−14.40° E 28.10° N	−15.50° E 28.10° N	$\sigma < 27.3$	−0.82/0.56	−0.9	Hernandez-Guerra et al., 2002
South Portugal	−8.70° E 37.60° N	−11.00° E 37.60° N	$\sigma < 27.25$ 27.25 < σ < 32.35	0.15/0.42 3.02/2.73	2.7−5.7 1.2−5.2	Jorge da Silva, 1996; Mazé et al., 1997; Coelho et al., 2002
Portugal	−20.00° E 40.10° N	−8.10° E 40.00° N	$\sigma < 27.7$ 27.7 < σ < 36.98 36.98 < σ < 45.85 45.85 < σ	1.07/0.61 1.35/3.17 0.27/1.32 0.68/0.54	0.5−2.8 −1.4−0.5 −1.3−0.5 0.8−1.6	Alvarez et al., 2004; Lherminier et al., 2007

Table 2a. Continued.

	Ext. 1	Ext. 2	Transport classes	Model values Mean/StdDev	Published Estimations	References
Galicia	-9.10° E 43.00° N	-10.50° E 43.00° N	$\sigma < 27.25$ 27.25 < $\sigma < 32.35$ $z < 400$ $400 < z < 900$ $900 < z < 1500$	0.32/0.33 3.63/1.66 1.71/1.11 1.72/0.69 1.23/0.81	1.31-4.7 0.42-1.8 0.9 0.7 0.2	Jorge da Silva, 1996; Mazé et al., 1997; Mauritzen et al., 2001; Coelho et al., 2002
Celtic shelf	-10.10° E 47.60° N	-9.40° E 48.40° N	$200 < z < 1500$ 200 < z < 3000	4.31/2.85 4.71/3.49	1 3	Pingree and Le Cann, 1990
Biscay	-4.00° E 48.20° N	-8.10° E 43.10° N	$S < 35$ 35 < S < 35.6 $35.6 < S$	-024/0.31 0.04/0.31 0.23/0.55	-0.1-0.1 -0.2-0.0 -2.6--2.0	Frail-Nuez et al., 2008
Ellett line	-7.70° E 56.80° N	-13.80° E 57.50° N	$z < 500$ z < 1200 $1200 < z < 1800$	2.86/0.54 3.89/0.93 -0.19/0.09	2.5-2.7 3.5-3.7 0.2	Ellett and Martin, 1973; Holliday et al., 2000
St. Georges Channel	-6.45° E 52.30° N	-5.10° E 51.80° N	NO	0.08/0.06	0.18	Brown et al., 2003
North Irish Sea Channel	-5.00° E 54.90° N	-5.60° E 54.60° N	NO	0.01/0.05	-0.175-0.14	Howarth, 1982; Brown and Gmitrowitz, 1995
Dover Strait	1.80° E 50.90° N	1.35° E 51.20° N	NO	0.07/0.06	0.094-0.17	Otto et al., 1990; Prandle et al., 1996
Faeroe Bank Channel	-7.00° E 61.80° N	-8.50° E 61.00° N	$T < 0$ T < 3 NO	-0.0/0.00 -1.23/0.22 -3.10/0.44	-1.5--0.5 -2.8--1.0 -2.8--0.5	Saunders, 1990; Krauss, 1995; Van Aken and Becker, 1996
Wyville Thomson Ridge	-8.80° E 60.50° N	-6.50° E 59.70° N	$T < 0$ T < 3 NO	0.00/0.00 0.03/0.02 2.32/0.42	-0.3--0.06 -0.35--0.1 -1.0--0.2	Ellett et al., 1986; Saunders, 1990; Van Aken and Becker, 1996; Hansen and Østerhus, 2000; Sherwin and Turrell, 2005
Faeroe Shetland Channel	-6.60° E 61.40° N	-3.50° E 60.10° N	$T < 0$ 0 < T	1.19/0.19 2.43/0.86	1.7--1.5 2.0-3.8	Saunders, 1990; Krauss, 1995; Van Aken and Becker, 1996; Østerhus et al., 2005
North Faeroe	-6.10° E 62.30° N	-6.10° E 65.00° N	NO	5.12/1.59 -1.03/0.42	2.9-5.0 -3.2	Krauss, 1995; Saunders, 1996; Van Aken and Becker, 1996; Hansen et al., 1998
Scotland-Shetland	-3.10° E 58.60° N	-1.30° E 60.00° N	NO	0.36/0.21	0.3-0.4	Otto et al., 1990
Shetland-Norway Trench	-1.30° E 59.90° N	3.70° E 59.90° N	NO	-0.70/0.26	-0.6	Otto et al., 1990
Norway Trench-Norway	3.70° E 59.90° N	5.10° E 59.90° N	NO	1.24/0.44	1.8	Otto et al., 1990
Skagerrak	10.08° E 60.00° N	10.08° E 57.00° N	NO	1.31/0.30	0.5-2.1	Rydberg et al., 1996; Rodhe, 1996
Kattegat	10.00° E 57.00° N	13.00° E 57.00° N	NO	0.02/0.02	0.055	Andersson and Rydberg, 1993

**NEMO on the shelf:
assessment of the
Iberia–Biscay–Ireland
configuration**

C. Maraldi et al.

Title Page

Abstract Introduction

Conclusions References

Tables Figures

⏪ ⏩

⏴ ⏵

Back Close

Full Screen / Esc

Printer-friendly Version

Interactive Discussion



NEMO on the shelf: assessment of the Iberia–Biscay–Ireland configuration

C. Maraldi et al.

Table 2b. Heat flux estimates from the model and the literature. Model transports are estimated from monthly fields and mean and RMS values are presented. Units are TW.

	Ext. 1	Ext. 2	Transport classes	Model values Mean/RMS	Published Estimations	References
Faeroe Shetland Channel	–6.60° E 61.40° N	–3.50° E 60.10° N	0 < T	117.17/33.36	123–156	Turrell et al., 2003; Østerhus et al., 2005
North Faeroe	–6.10° E 62.30° N	–6.10° E 65.00° N	0 < T	95.84/23.75	110–139	Hansen et al., 2003

Title Page

Abstract

Introduction

Conclusions

References

Tables

Figures

◀

▶

◀

▶

Back

Close

Full Screen / Esc

Printer-friendly Version

Interactive Discussion



NEMO on the shelf: assessment of the Iberia–Biscay–Ireland configuration

C. Maraldi et al.

Table 2c. Freshwater flux estimates from the model and the literature. Model transports are estimated from monthly fields and mean and RMS values are presented. Units are kT s^{-1} .

	Ext. 1	Ext. 2	Transport classes	Model values Mean/RMS	Published Estimations	References
Faeroe Shetland Channel	–6.60° E 61.40° N	–3.50° E 60.10° N	$0 < T$	86.55/30.51	115–139	Turrell et al., 2003; Østerhus et al., 2005
North Faeroe	–6.10° E 62.30° N	–6.10° E 65.00° N	$0 < T$	123.88/34.69	115–143	Hansen et al., 2003

Title Page

Abstract

Introduction

Conclusions

References

Tables

Figures

◀

▶

◀

▶

Back

Close

Full Screen / Esc

Printer-friendly Version

Interactive Discussion



NEMO on the shelf: assessment of the Iberia–Biscay–Ireland configuration

C. Maraldi et al.

Table 3. RMS error of the complex amplitude difference between observed and modelled tidal components.

Regional	M2	S2	K1	O1	M4
Global	21.6	8.0	1.8	1.3	7.1
Canary	2.8	1.7	0.4	0.2	0.1
Mediterranean Sea	3.3	0.7	0.9	0.2	0.4
Gibraltar	6.4	1.7	0.8	0.5	1.0
Gulf of Cadiz and West Iberian Plateau	3.2	3.4	0.9	0.4	0.6
Bay of Biscay	29.5	10.6	1.2	0.8	0.8
Irish Sea	25.9	10.1	1.7	1.3	11.1
English Channel	23.6	8.1	1.5	1.9	7.5
North Sea	14.7	4.7	2.7	1.0	6.2
Baltic	29.8	9.0	2.4	2.1	0.9

[Title Page](#)
[Abstract](#)
[Introduction](#)
[Conclusions](#)
[References](#)
[Tables](#)
[Figures](#)
[⏪](#)
[⏩](#)
[◀](#)
[▶](#)
[Back](#)
[Close](#)
[Full Screen / Esc](#)
[Printer-friendly Version](#)
[Interactive Discussion](#)


NEMO on the shelf: assessment of the Iberia–Biscay–Ireland configuration

C. Maraldi et al.

[Title Page](#)
[Abstract](#)
[Introduction](#)
[Conclusions](#)
[References](#)
[Tables](#)
[Figures](#)
[⏪](#)
[⏩](#)
[◀](#)
[▶](#)
[Back](#)
[Close](#)
[Full Screen / Esc](#)
[Printer-friendly Version](#)
[Interactive Discussion](#)


Table 4. RMS between observed and modelled tidal ellipse parameters.

	SEMA	SEMI	Inc	Pha
Barotropic ellipses (M_2)				
IBI domain	4.8	3.9	23.8	27.0
Gibraltar	13.3	5.6	8.3	26.4
Portugal Plateau	4.2	0.4	31.6	22.6
Armorican and Celtic Shelves	4.1	6.9	33.7	45.5
North Sea	3.3	2.3	9.5	9.0
Irish Sea	5.3	3.0	3.0	3.9
Baroclinic ellipses (buoys, M_2)				
IBI domain	4.4	2.6	22.1	31.3
Baroclinic ellipses (radar, M_2)				
Iroise sea (depth > 50 m)	4.6	2.5	5.1	5.6
Baroclinic ellipses (radar, M_4)				
Iroise sea (depth > 50 m)	1.1	0.3	17.1	39.6

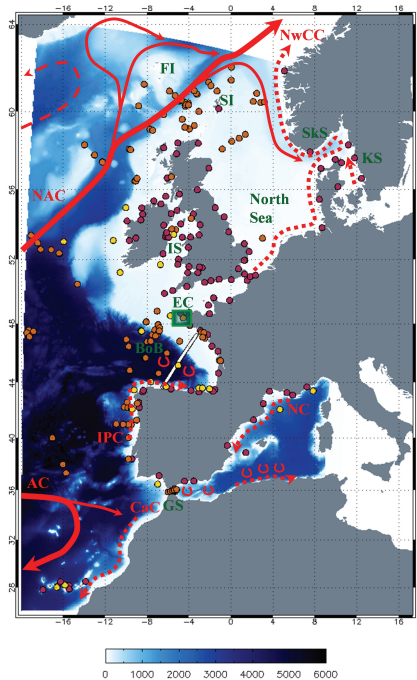


Fig. 1. Bathymetry of the domain (in meter). Superposed are the tide gauge positions (red dots), the buoy locations (yellow dots), the current meter data for tidal comparisons (orange dots), the altimeter track crossing the Bay of Biscay (white line) and the area covered by the HF radar for surface current measurements off West Brittany (green box). The main surface dynamical features are also shown: the Azores Current (AC), the Canary Current (CaC), the Northern Current (NC), the Iberian Poleward Current (IPC), the Norwegian Coastal Current (NwCC), the North Atlantic Current (NAC). Red symbols represent mesoscale activity in the Mediterranean Sea and in the Bay of Biscay. Some geographical features of the area are also mentioned: the Gibraltar Strait (GS), the Bay of Biscay (BoB), the English Channel (EC), the Irish Sea (IS), the Shetland Islands (SI) and the Faeroe Islands (FI), the Skagerrak Strait (SkS) and the Kattegat Strait (KS).

**NEMO on the shelf:
assessment of the
Iberia–Biscay–Ireland
configuration**

C. Maraldi et al.

Title Page	
Abstract	Introduction
Conclusions	References
Tables	Figures
⏪	⏩
◀	▶
Back	Close
Full Screen / Esc	
Printer-friendly Version	
Interactive Discussion	



**NEMO on the shelf:
assessment of the
Iberia–Biscay–Ireland
configuration**

C. Maraldi et al.

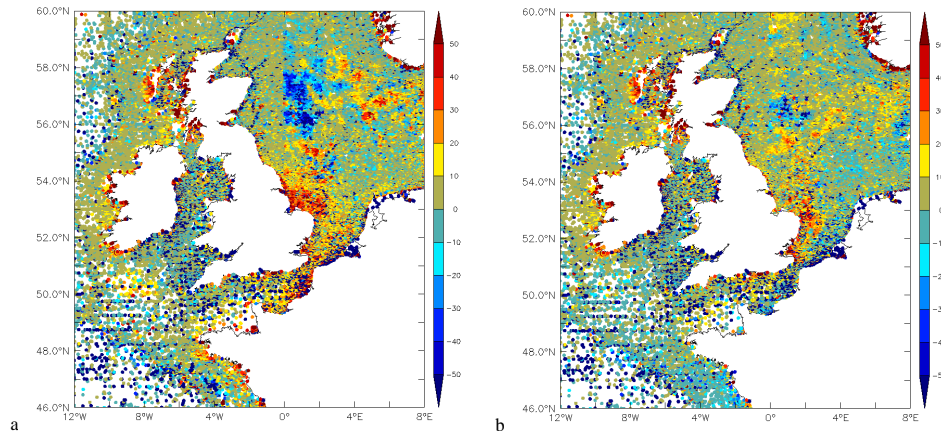


Fig. 2. Comparisons of the bathymetry GEBCO08 (a) and the new bathymetry used in the model (b) with ICES profile depth. The results represent percentage of error between data and bathymetry grids. ICES depth is deduced from ICES measurements by taking the difference between the deepest and the shallowest measurements.

Title Page

Abstract

Introduction

Conclusions

References

Tables

Figures



Back

Close

Full Screen / Esc

Printer-friendly Version

Interactive Discussion

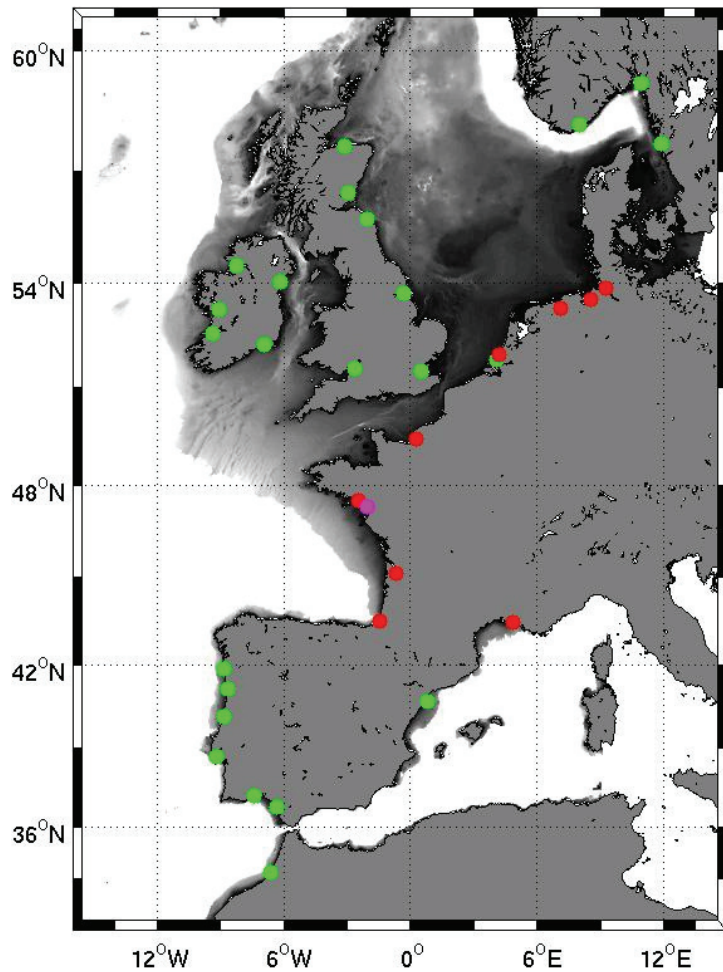


Fig. 3. Runoffs of the IBI configuration.

**NEMO on the shelf:
assessment of the
Iberia–Biscay–Ireland
configuration**

C. Maraldi et al.

Title Page

Abstract Introduction

Conclusions References

Tables Figures

⏪ ⏩

◀ ▶

Back Close

Full Screen / Esc

Printer-friendly Version

Interactive Discussion



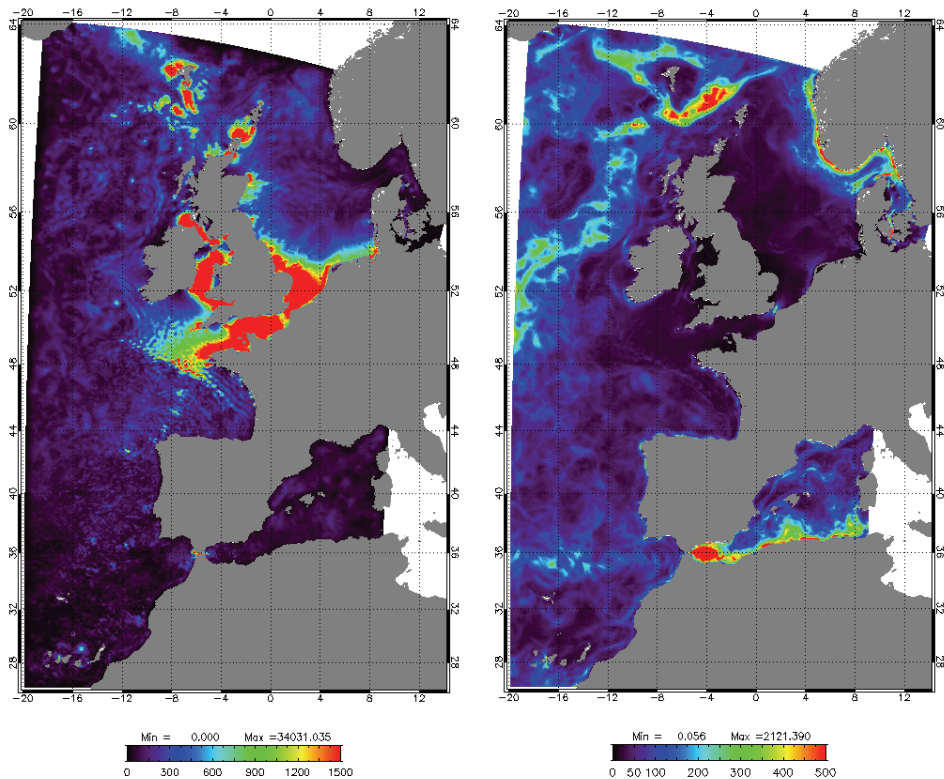


Fig. 4. Surface EKE for periods below 25 h **(a)** and for periods above 25 h **(b)**. **(a)** is computed over July 2008 and **(b)** is computed over year 2008.

**NEMO on the shelf:
assessment of the
Iberia–Biscay–Ireland
configuration**

C. Maraldi et al.

Title Page	
Abstract	Introduction
Conclusions	References
Tables	Figures
⏪	⏩
◀	▶
Back	Close
Full Screen / Esc	
Printer-friendly Version	
Interactive Discussion	



NEMO on the shelf: assessment of the Iberia–Biscay–Ireland configuration

C. Maraldi et al.

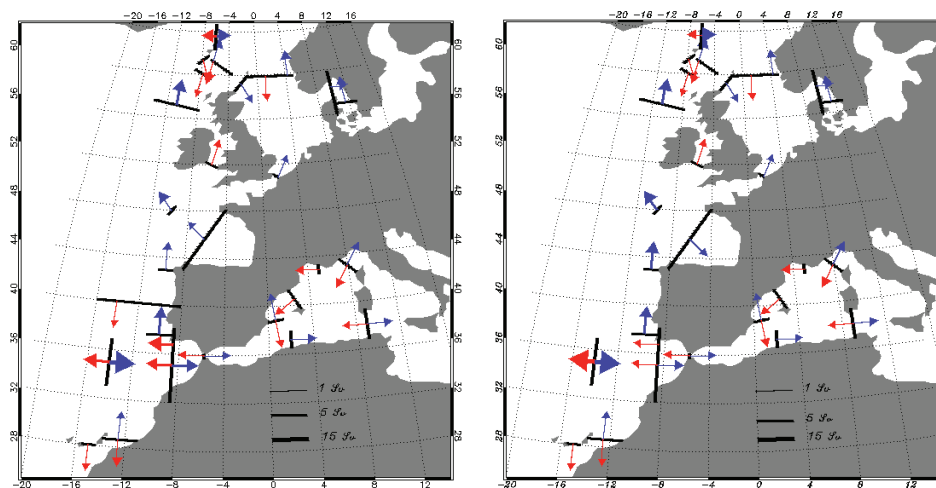


Fig. 5. Transport estimates from the literature **(a)** and from monthly model fields **(b)**. The thickness of the arrow indicates the volume in Sv. The blue color (resp. red color) indicates northward (resp. southward) transports or eastward (westward) transport for zonal sections as computed from observations. Estimations used for the plot are in bold in Table 2a. Model transports corresponding to the estimations computed from observations are plotted using the same color than published estimations.

Title Page

Abstract

Introduction

Conclusions

References

Tables

Figures

◀

▶

◀

▶

Back

Close

Full Screen / Esc

Printer-friendly Version

Interactive Discussion

NEMO on the shelf: assessment of the Iberia–Biscay–Ireland configuration

C. Maraldi et al.

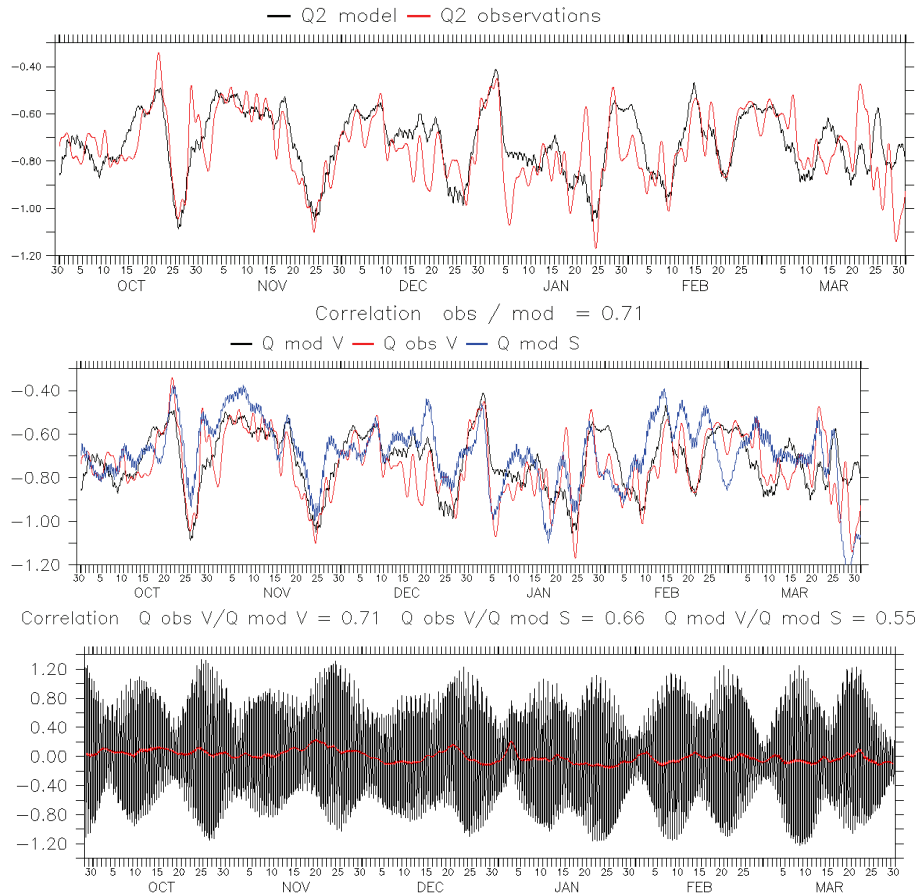
[Title Page](#)
[Abstract](#)
[Introduction](#)
[Conclusions](#)
[References](#)
[Tables](#)
[Figures](#)
[◀](#)
[▶](#)
[◀](#)
[▶](#)
[Back](#)
[Close](#)
[Full Screen / Esc](#)
[Printer-friendly Version](#)
[Interactive Discussion](#)


Fig. 6. Transports (outflow) at Gibraltar Strait for QobsV, QmodV and QmodS (a). Depth of the interface for QmodV and QmodS (b). Unfiltered sea surface elevations (e.g. includes tidal elevations) in black and 2-day low-pass filter sea surface elevations in red at the Gibraltar Strait (c).

NEMO on the shelf: assessment of the Iberia–Biscay–Ireland configuration

C. Maraldi et al.

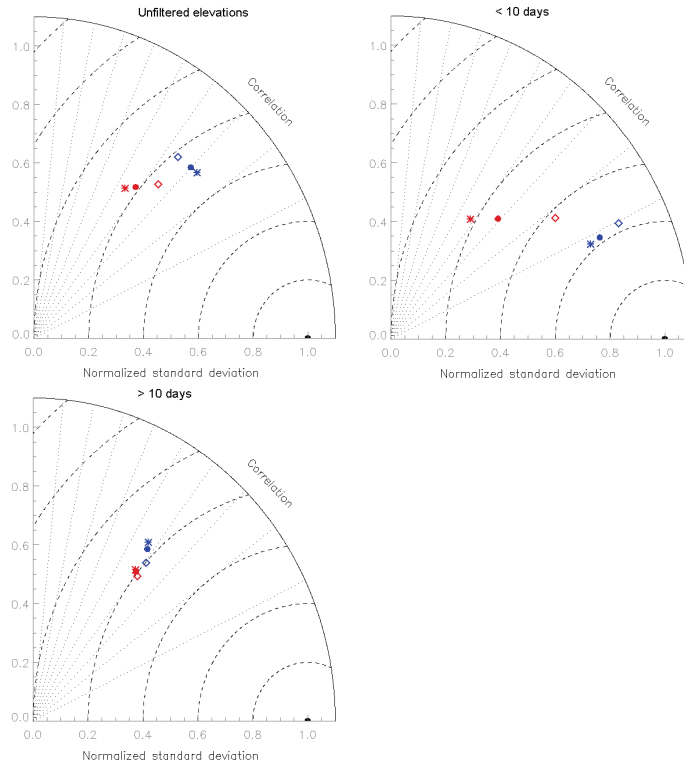


Fig. 7. Taylor diagram for comparisons between tide gauge data and the model residual elevations (blue) and the inverse barometer (red). The radial coordinate indicates the standard deviation normalized by the data standard deviation and the angular coordinate represents the correlation with observations. The observations are indicated with the black point and distances between the colored model points and the data point indicate the RMS difference error. Plain dots are for the whole area, stars are for locations north of 50° N and diamonds are for locations south of 50° N. Results are shown for the unfiltered time series (a), for periods below 10 days (b) and for periods above 10 days (c).

[Title Page](#)
[Abstract](#)
[Introduction](#)
[Conclusions](#)
[References](#)
[Tables](#)
[Figures](#)
[⏪](#)
[⏩](#)
[◀](#)
[▶](#)
[Back](#)
[Close](#)
[Full Screen / Esc](#)
[Printer-friendly Version](#)
[Interactive Discussion](#)

NEMO on the shelf: assessment of the Iberia–Biscay–Ireland configuration

C. Maraldi et al.

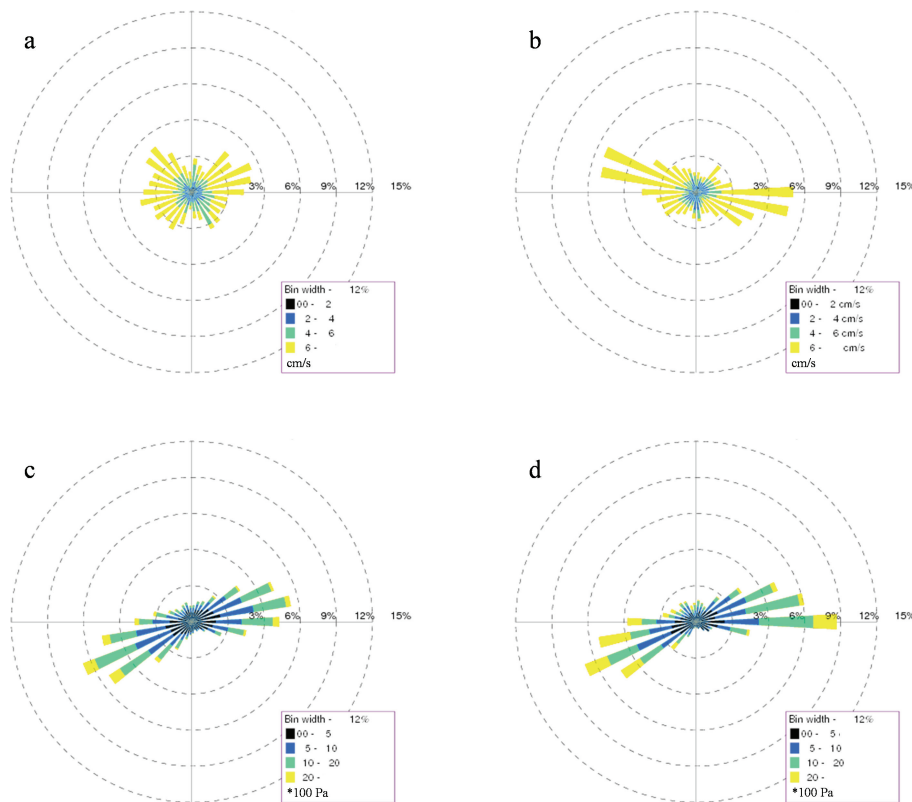


Fig. 8. Wind rose of the 2-day low pass filtered residual currents as observed **(a)** and modelled **(b)** at the Estaca de Bares buoy station. Corresponding wind stress as observed at the buoy station **(c)** and as extracted from the model forcing fields using ECMWF wind speed **(d)**.

Title Page

Abstract

Introduction

Conclusions

References

Tables

Figures

◀

▶

◀

▶

Back

Close

Full Screen / Esc

Printer-friendly Version

Interactive Discussion

NEMO on the shelf: assessment of the Iberia–Biscay–Ireland configuration

C. Maraldi et al.

Title Page

Abstract

Introduction

Conclusions

References

Tables

Figures

◀

▶

◀

▶

Back

Close

Full Screen / Esc

Printer-friendly Version

Interactive Discussion

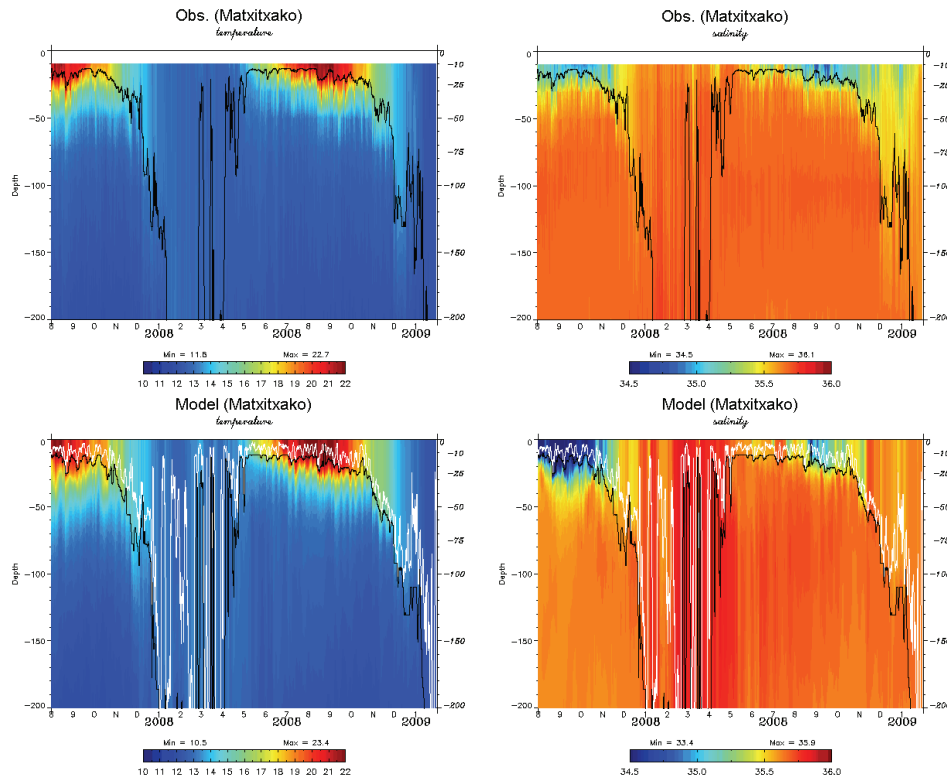


Fig. 10. Temperature and salinity at station Matixxako from the observations **(a, b)** and from the model **(c, d)**. The mixed layer depth is also represented with a white line. It is computed as the depth at which the density change from the surface density is 0.01. It is not represented on the observation plots as the observation shallowest depth is 10 m. The black line represents the depth at which the density change from the 10 m density is 0.01.

NEMO on the shelf: assessment of the Iberia–Biscay–Ireland configuration

C. Maraldi et al.

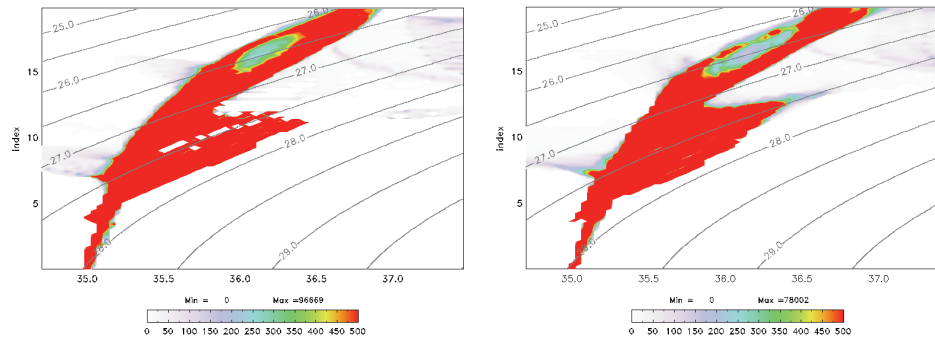


Fig. 11. Volumetric TS diagram (10^3 m^3) for the ARIVO climatology **(a)** and for the model **(b)** over the IBI domain. The diagram is presented for bathymetry depth deeper than 200 m. The data are yearly averaged and the model thermohaline fields are averaged over 2008.

Title Page

Abstract

Introduction

Conclusions

References

Tables

Figures

◀

▶

◀

▶

Back

Close

Full Screen / Esc

Printer-friendly Version

Interactive Discussion

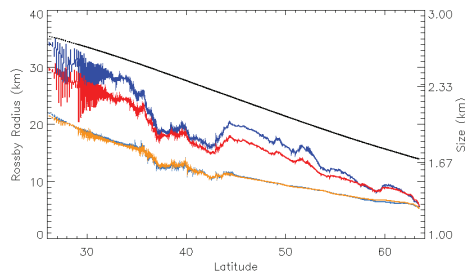
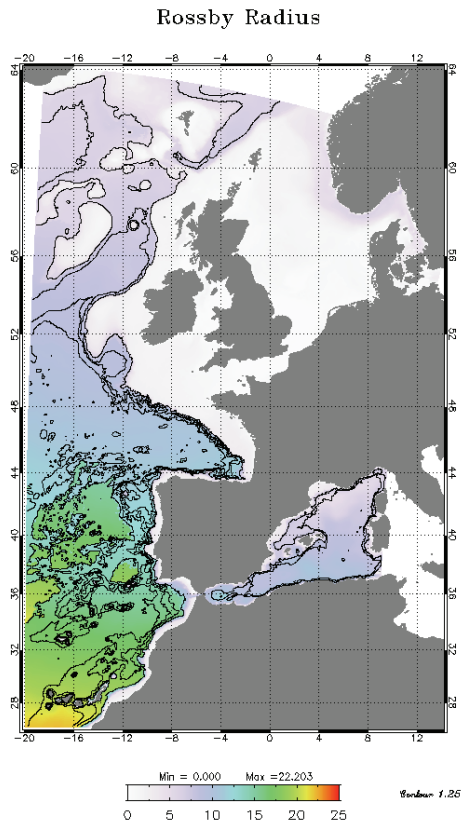


Fig. 12. (a) First Rossby radius of deformation for the model (in km). **(b)** First Rossby radius as a function of latitude. The radius is averaged for bathymetry points deeper than 1000 m. We distinguish two cases: 1) N is integrated over the full water depth as in the formula of Chelton et al. (1998) for the model (dark blue) and the climatology (red), 2) N is integrated over the upper 1500 m for the model (light blue) and the climatology (orange). We also show the variations of the grid size with latitude (black line).

**NEMO on the shelf:
assessment of the
Iberia–Biscay–Ireland
configuration**

C. Maraldi et al.

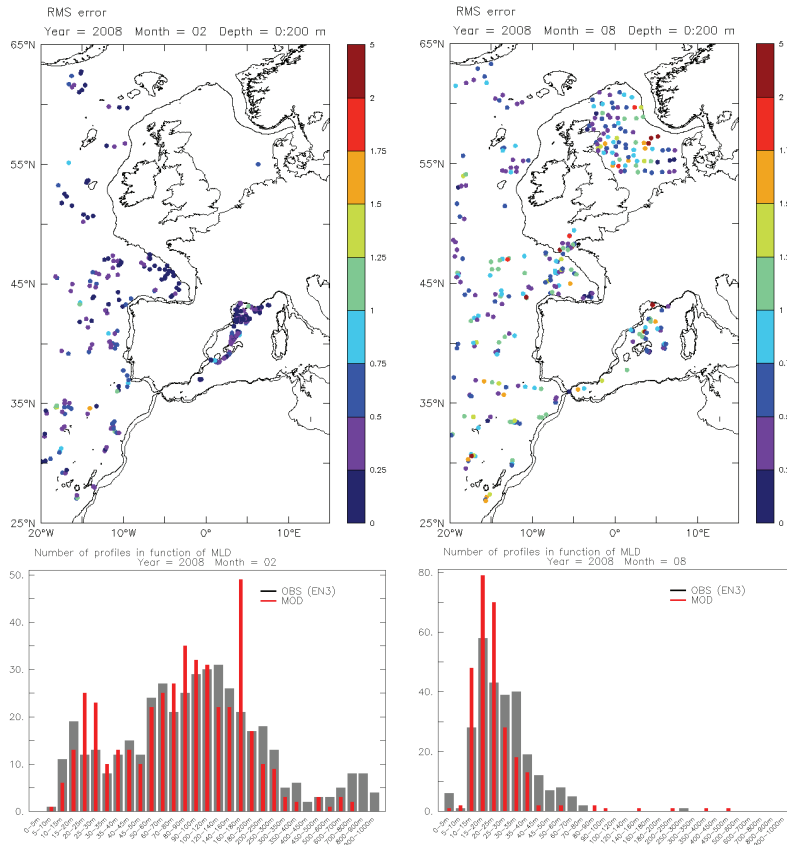


Fig. 13. RMS of temperature differences between EN3 profiles and model profiles computed over the first 200 m. Results are presented for February 2008 (a) and August 2008 (b). Distribution of profiles in different mixed layer depth ranges computed from EN3 data (grey) and model fields (red) for February 2009 (c) and August 2008 (d).

Title Page

Abstract Introduction

Conclusions References

Tables Figures

◀ ▶

◀ ▶

Back Close

Full Screen / Esc

Printer-friendly Version

Interactive Discussion



NEMO on the shelf: assessment of the Iberia–Biscay–Ireland configuration

C. Maraldi et al.

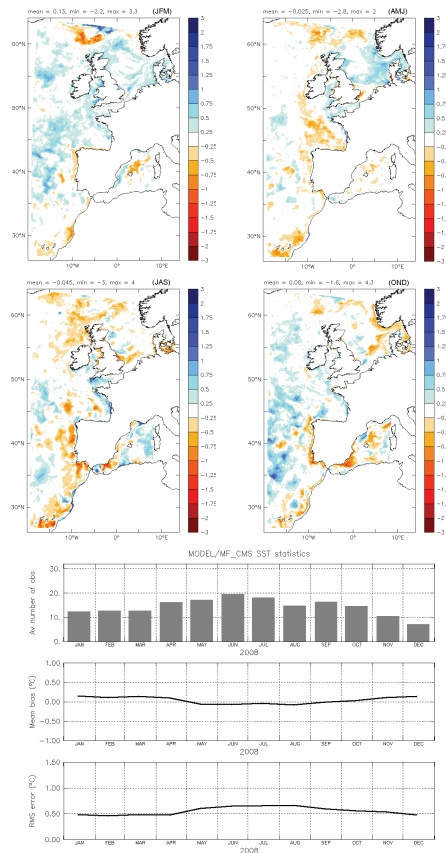


Fig. 14. Map of mean bias between Météo-France/CMS satellite data and model SST over January–March 2008 (a), April–June 2008 (b), July–September 2008 (c) and October–December 2008 (d). Negative bias indicates that the model is too cold. (e) Number of observations, monthly bias and RMS over the whole IBI area. Units are in °C.

**NEMO on the shelf:
assessment of the
Iberia–Biscay–Ireland
configuration**

C. Maraldi et al.

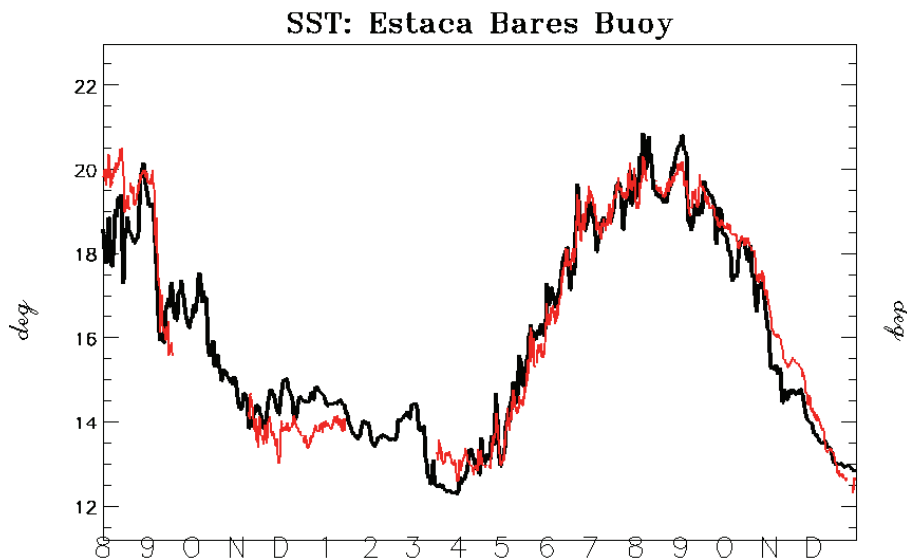


Fig. 15. Modelled (black) and observed (red) sea surface temperatures at the Estaca de Bares buoy station ($44^{\circ} 3.6' \text{ N}$ – $7^{\circ} 37.2' \text{ W}$) from August 2008 to December 2009. Note that there is no data during September–October 2007 and January–March 2008.

[Title Page](#)[Abstract](#)[Introduction](#)[Conclusions](#)[References](#)[Tables](#)[Figures](#)[⏪](#)[⏩](#)[⏴](#)[⏵](#)[Back](#)[Close](#)[Full Screen / Esc](#)[Printer-friendly Version](#)[Interactive Discussion](#)

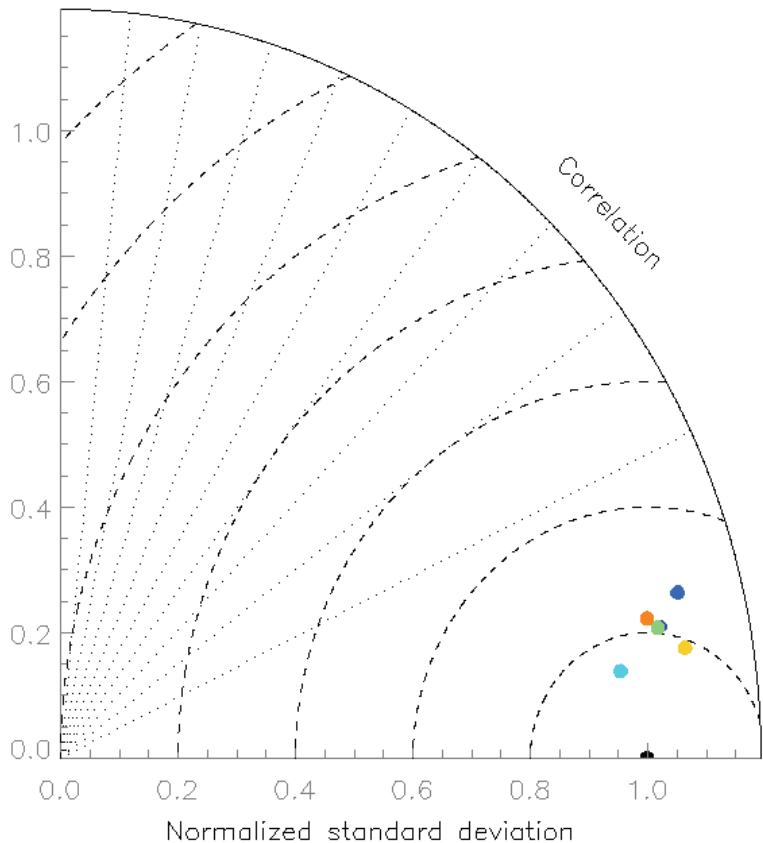


Fig. 16. Taylor diagram of the 1-day low pass filtered SST at buoy locations. The dark blue point is for comparisons within the whole domain, the turquoise blue point for the Canary region, the light blue point for the Mediterranean Sea, the light green point for the Iberian Peninsula region, the yellow point for the Bay of Biscay and the orange point for the Celtic sea and the Irish sea.

**NEMO on the shelf:
assessment of the
Iberia–Biscay–Ireland
configuration**

C. Maraldi et al.

Title Page	
Abstract	Introduction
Conclusions	References
Tables	Figures
⏪	⏩
◀	▶
Back	Close
Full Screen / Esc	
Printer-friendly Version	
Interactive Discussion	



**NEMO on the shelf:
assessment of the
Iberia–Biscay–Ireland
configuration**

C. Maraldi et al.

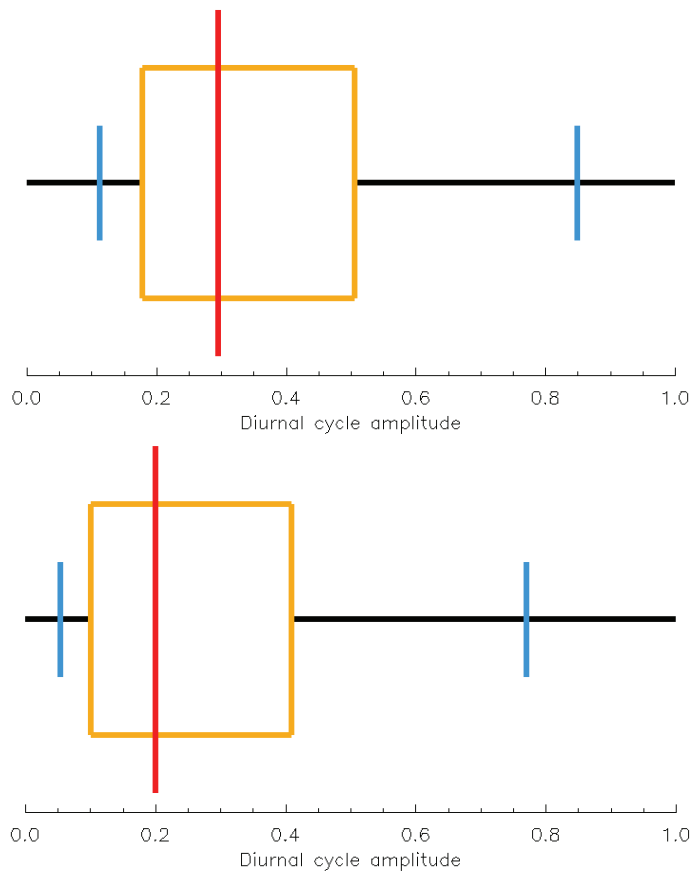


Fig. 17. Boxplot of the diurnal cycle computed from data **(a)** and from model **(b)**. The distribution is described with percentiles of data (vertical lines). From the left to the right we indicate the position of the 10th percentile (blue), the lower quartile (yellow), the median (red), the upper quartile (yellow) and the 90th percentile (blue).

[Title Page](#)[Abstract](#)[Introduction](#)[Conclusions](#)[References](#)[Tables](#)[Figures](#)[◀](#)[▶](#)[◀](#)[▶](#)[Back](#)[Close](#)[Full Screen / Esc](#)[Printer-friendly Version](#)[Interactive Discussion](#)

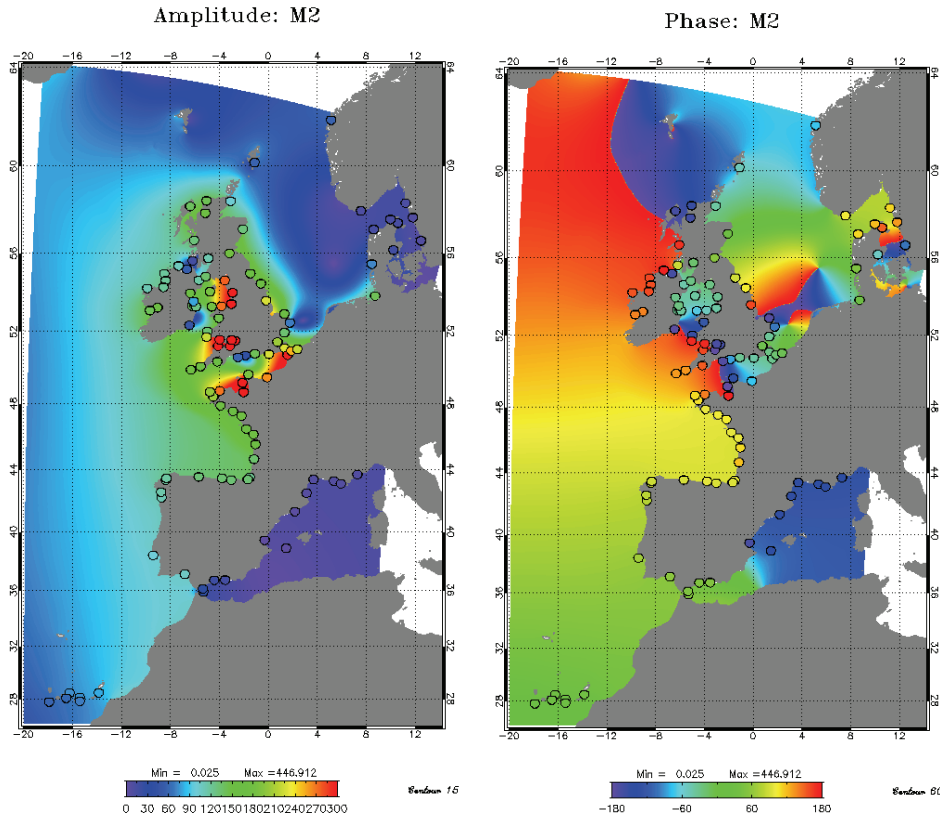


Fig. 18. Amplitude in cm **(a)** and phase in degrees **(b)** of the M_2 tidal constituent computed from the model over the whole domain. Overplotted filled dots represent the M_2 observed harmonic constants. Differences of amplitude **(c)** and phase **(d)** between the FES2004 solution and the model for the M_2 constituent. Overplotted filled dots represent amplitude and phase differences between tide gauges and the model.

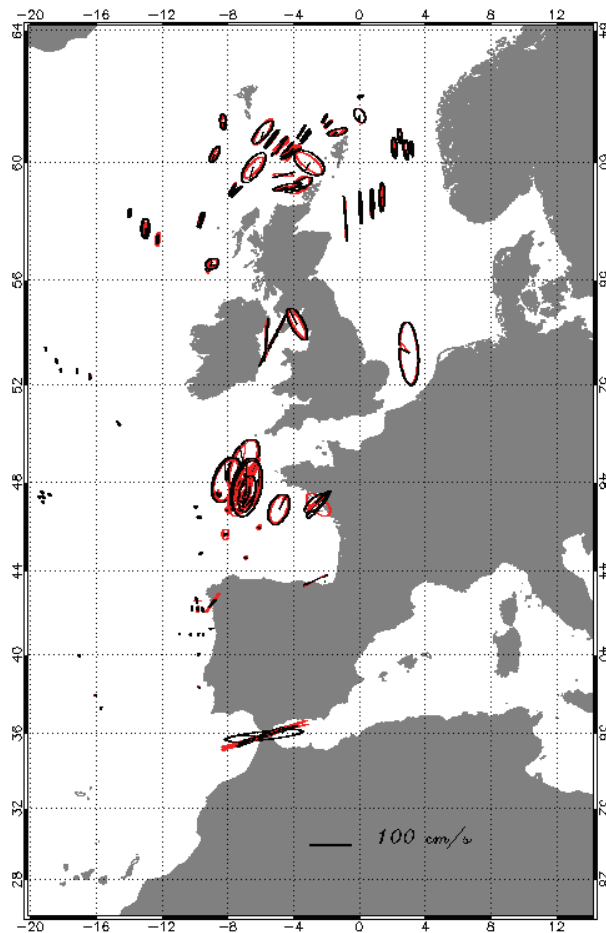


Fig. 19. Modelled (black) and observed (red) M_2 barotropic tidal ellipses. Observations encompass historical data from BODC, BSH and data collected within the framework of the WOCE experiment.

**NEMO on the shelf:
assessment of the
Iberia–Biscay–Ireland
configuration**

C. Maraldi et al.

Title Page

Abstract Introduction

Conclusions References

Tables Figures

⏪ ⏩

◀ ▶

Back Close

Full Screen / Esc

Printer-friendly Version

Interactive Discussion



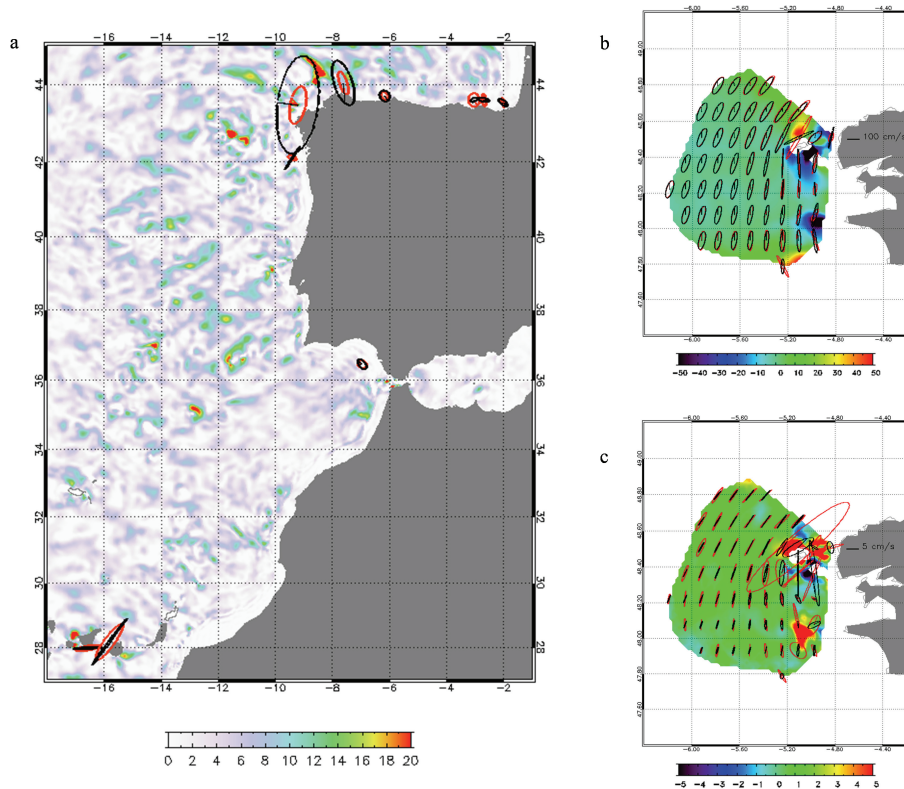


Fig. 20. (a) Modelled (black) and observed (red) surface tidal ellipses at buoy locations for the M_2 component. The map represents the difference of the M_2 surface velocity amplitudes between the run with stratification (run_{bc}) and the run without stratification (run_{bt}). (b, c) Modelled (black) and radar (red) surface tidal ellipses for the M_2 and the M_4 components. The map represents the difference between the observed and modelled semi major axis ($cm\ s^{-1}$).

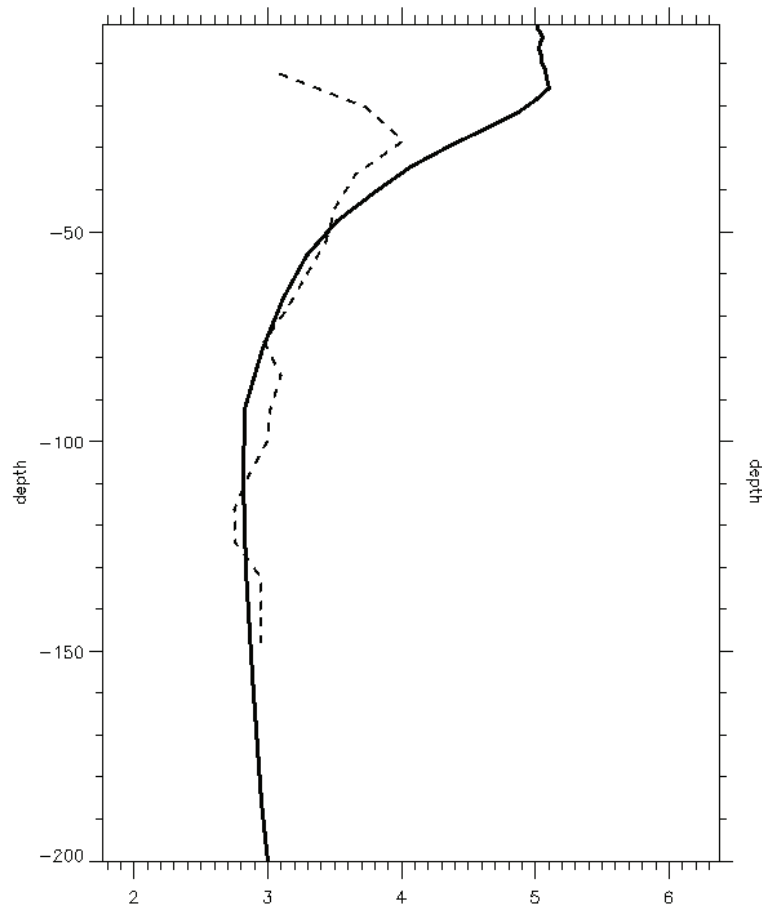


Fig. 21. Vertical profiles of the M2 semi major axis as observed (dashed line) and modelled (full line) at the Matxitxako buoy location.

**NEMO on the shelf:
assessment of the
Iberia–Biscay–Ireland
configuration**

C. Maraldi et al.

Title Page	
Abstract	Introduction
Conclusions	References
Tables	Figures
◀	▶
◀	▶
Back	Close
Full Screen / Esc	
Printer-friendly Version	
Interactive Discussion	



**NEMO on the shelf:
assessment of the
Iberia–Biscay–Ireland
configuration**

C. Maraldi et al.

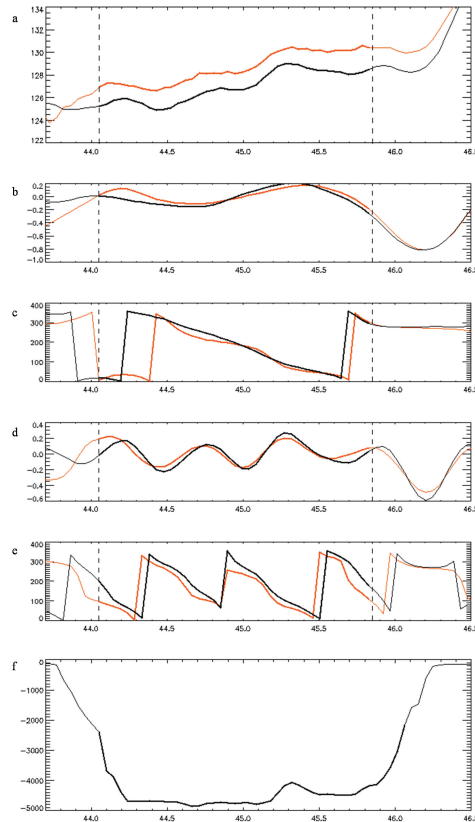


Fig. 22. (a) Along track amplitudes (cm) deduced from the M_2 harmonic analysis of altimetric data (red) and model (black). (b) Baroclinic amplitudes in cm and (c) phase of the residual tides for the altimetric data (red) and the model (black) and for the first baroclinic mode. (d) Baroclinic amplitudes in cm and (e) phase of the residual tides for the altimetric data (red) and the model (black) and for the second baroclinic mode. (f) Along track bathymetry (m).

Title Page

Abstract

Introduction

Conclusions

References

Tables

Figures

◀

▶

◀

▶

Back

Close

Full Screen / Esc

Printer-friendly Version

Interactive Discussion

**NEMO on the shelf:
assessment of the
Iberia–Biscay–Ireland
configuration**

C. Maraldi et al.

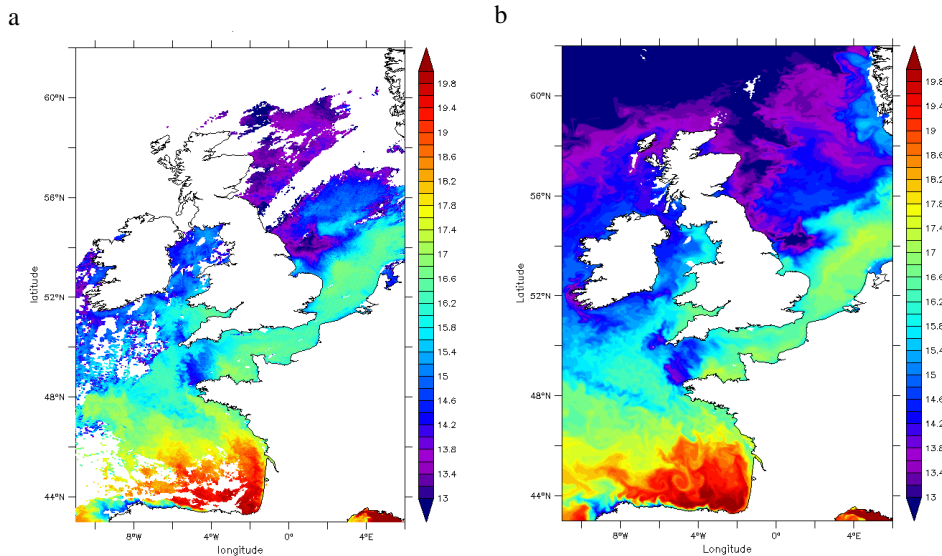


Fig. 23. Sea surface temperature ($^{\circ}\text{C}$) from MODIS data **(a)** and from the model **(b)** on 27 September 2008.

Title Page

Abstract

Introduction

Conclusions

References

Tables

Figures

◀

▶

◀

▶

Back

Close

Full Screen / Esc

Printer-friendly Version

Interactive Discussion

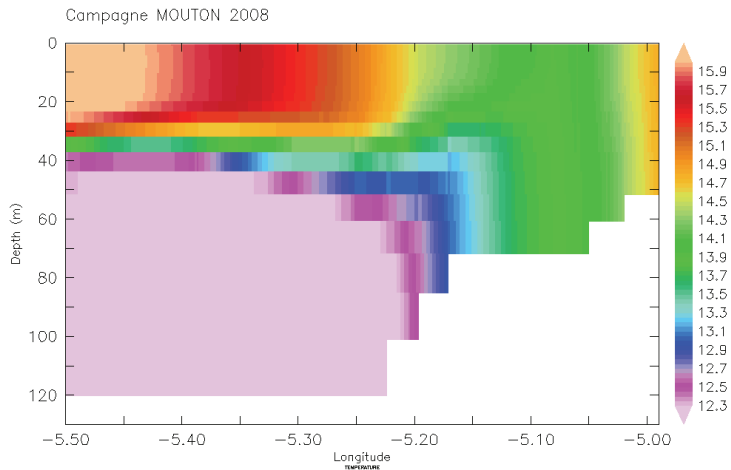
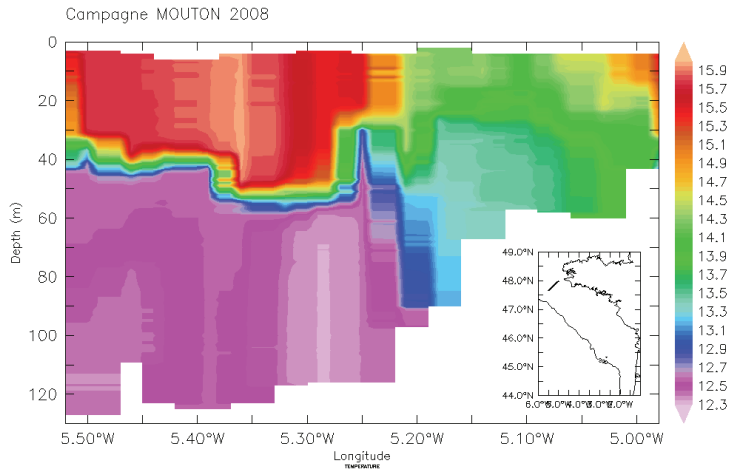


Fig. 24. Temperature ($^{\circ}\text{C}$) transect crossing the Ushant front as observed during the MOUTON cruise **(a)** and as modelled in IBI **(b)** on the 1 October 2008.

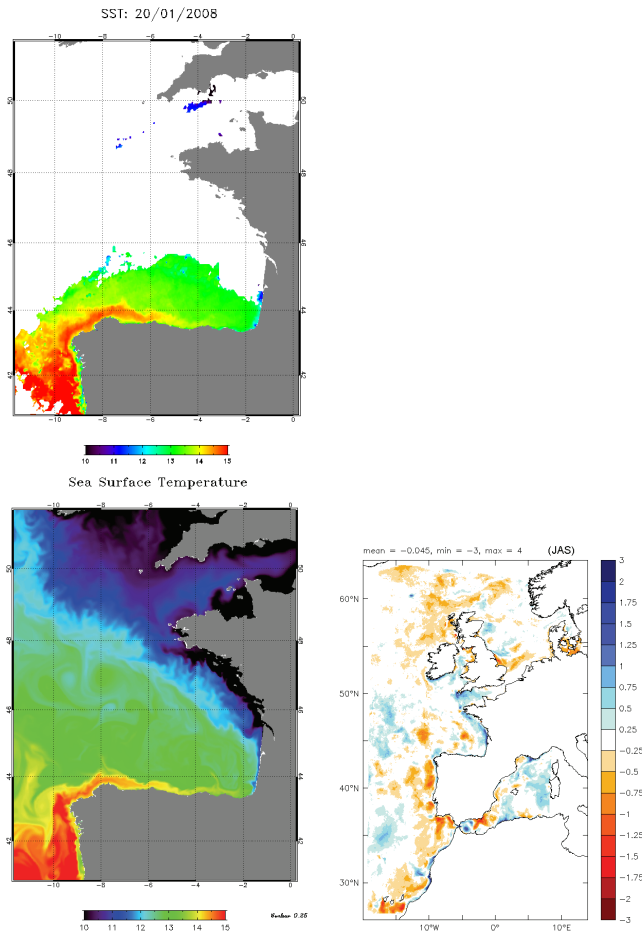


Fig. 25. Sea surface temperature ($^{\circ}\text{C}$) from AVHRR data **(a)** and from the model **(b)** the 20 January 2008. Modelled temperature at 200 m the 20 January 2008 **(c)**.

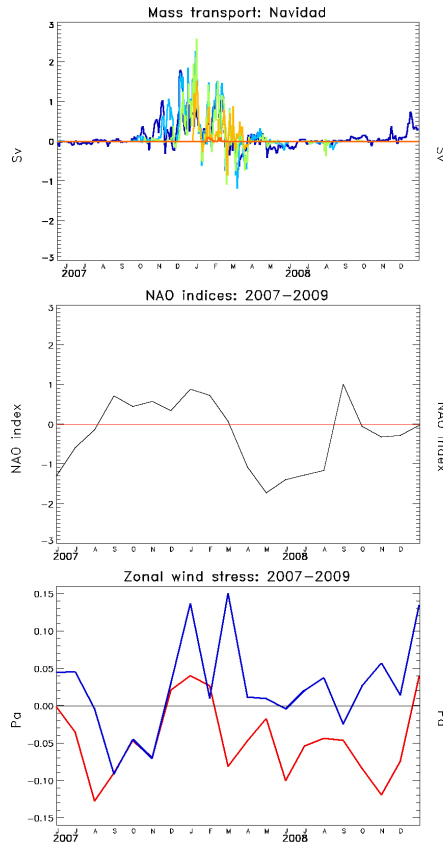


Fig. 26. (a) Transport of the poleward flow for water mass warmer than 13.0 °C and saltier than 35.7 psu at 43.24° N (blue), at 7.61° W (turquoise blue), at 6.2° W (green), at 3.8° W (yellow) and at 44.4° N (orange). **(b)** NAO index. **(c)** Meridional wind stress τ_y off Western Iberia (red) and of the zonal wind stress τ_x off Northern Iberia. Boxes (blue). Boxes chosen for the spatial average of τ_x and τ_y have been chosen following the study of Le Cann and Serpette (2009).

**NEMO on the shelf:
assessment of the
Iberia–Biscay–Ireland
configuration**

C. Maraldi et al.

Title Page

Abstract Introduction

Conclusions References

Tables Figures

⏪ ⏩

◀ ▶

Back Close

Full Screen / Esc

Printer-friendly Version

Interactive Discussion

